



$\Delta O_2/N_2'$ as a New Tracer of Marine Net Community Production: Application and Evaluation in the Subarctic Northeast Pacific and Canadian Arctic Ocean

Robert W. Izett^{1*}, Roberta C. Hamme², Craig McNeil³, Cara C. M. Manning^{1,4,5}, Annie Bourbonnais⁶ and Philippe D. Tortell^{1,7}

¹ Department of Earth, Ocean and Atmospheric Sciences, University of British Columbia, Vancouver, BC, Canada, ² School of Earth and Ocean Sciences, University of Victoria, Victoria, BC, Canada, ³ Applied Physics Laboratory and School of Oceanography, University of Washington, Seattle, WA, United States, ⁴ Plymouth Marine Laboratory, Plymouth, United Kingdom, ⁵ National Centre for Earth Observation, Plymouth, United Kingdom, ⁶ School of the Earth, Ocean and Environment, University of South Carolina, Columbia, SC, United States, ⁷ Botany Department, University of British Columbia, Vancouver, BC, Canada

OPEN ACCESS

Edited by:

Jun Sun,
China University of Geosciences
Wuhan, China

Reviewed by:

Guilin Zhang,
Ocean University of China, China
Peter Leslie Croot,
National University of Ireland Galway,
Ireland

*Correspondence:

Robert W. Izett
robert_izett@live.com

Specialty section:

This article was submitted to
Marine Biogeochemistry,
a section of the journal
Frontiers in Marine Science

Received: 01 June 2021

Accepted: 28 June 2021

Published: 02 August 2021

Citation:

Izett RW, Hamme RC, McNeil C, Manning CCM, Bourbonnais A and Tortell PD (2021) $\Delta O_2/N_2'$ as a New Tracer of Marine Net Community Production: Application and Evaluation in the Subarctic Northeast Pacific and Canadian Arctic Ocean. *Front. Mar. Sci.* 8:718625. doi: 10.3389/fmars.2021.718625

We compared field measurements of the biological O_2 saturation anomalies, $\Delta O_2/Ar$ and $\Delta O_2/N_2$, from simultaneous oceanographic deployments of a membrane inlet mass spectrometer and optode/gas tension device (GTD). Data from the Subarctic Northeast Pacific and Canadian Arctic Ocean were used to evaluate $\Delta O_2/N_2$ as an alternative to $\Delta O_2/Ar$ for estimates of mixed layer net community production (NCP). We observed strong spatial coherence between $\Delta O_2/Ar$ and $\Delta O_2/N_2$, with small offsets resulting from differences in the solubility properties of Ar and N_2 and their sensitivity to vertical mixing fluxes. Larger offsets between the two tracers were observed across hydrographic fronts and under elevated sea states, resulting from the differential time-response of the optode and GTD, and from bubble dissolution in the ship's seawater lines. We used a simple numerical framework to correct for physical sources of divergence between N_2 and Ar, deriving the tracer $\Delta O_2/N_2'$. Over most of our survey regions, $\Delta O_2/N_2'$ provided a better analog for $\Delta O_2/Ar$, and thus more accurate NCP estimates than $\Delta O_2/N_2$. However, in coastal Arctic waters, $\Delta O_2/N_2$ and $\Delta O_2/N_2'$ performed equally well as NCP tracers. On average, mixed layer NCP estimated from $\Delta O_2/Ar$ and $\Delta O_2/N_2'$ agreed to within $\sim 2 \text{ mmol } O_2 \text{ m}^{-2} \text{ d}^{-1}$, with offsets typically smaller than other errors in NCP calculations. Our results demonstrate a significant potential to derive NCP from underway O_2/N_2 measurements across various oceanic regions. Optode/GTD systems could replace mass spectrometers for autonomous NCP derivation under many oceanographic conditions, thereby presenting opportunities to significantly expand global NCP coverage from various underway platforms.

Keywords: nitrogen, oxygen, net community production, gas dynamics, air-sea exchange, gas tracer, net community metabolism

INTRODUCTION

Marine net community production (NCP) represents the difference between gross photosynthesis and community-wide respiration, exerting a first-order control on the ocean's capacity to support upper trophic level biomass and sequester atmospheric carbon dioxide via the biological pump (Volk and Hoffert, 1985; Ware and Thomson, 2005). Accurately quantifying NCP is therefore important for understanding a variety of ecologically and economically important ocean processes, and for predicting climate-dependent shifts in marine biogeochemical cycles. Oceanic responses to climate change are likely to alter marine biological production (e.g., Moore et al., 2018), but our capacity to predict these changes is limited, in part, by poor data coverage. Multi-year NCP time-series are only available from a handful of deep ocean sites (Emerson, 2014), and many ship-based studies provide only sparse coverage in well-sampled ocean regions. New observational tools are thus required to facilitate NCP quantification on global scales and thereby enable predictions of its climate-related variability.

A common approach to estimating NCP involves quantification of the mixed layer O_2 mass balance, using O_2 measurements from ship-board surveys, moorings, profiling floats or gliders (e.g., Kaiser et al., 2005; Emerson and Stump, 2010; Bushinsky and Emerson, 2015; Palevsky and Nicholson, 2018). Since the O_2 saturation state is sensitive to both biological and physical processes, including temperature and salinity-dependent solubility effects and bubble injection, O_2 measurements alone are insufficient to accurately resolve NCP. To address this limitation, O_2 concentrations can be normalized to argon (Ar), a biologically inert gas with solubility properties that are virtually identical to O_2 (Craig and Hayward, 1987). The so-called “biological O_2 saturation anomaly,” $\Delta O_2/Ar$ (Eq. 1), defined by normalizing the seawater O_2/Ar ratio ($[O_2/Ar]_{sw}$) to the equilibrium ratio ($[O_2/Ar]_{eq}$), thus isolates the biological processes affecting O_2 .

$$\Delta O_2/Ar = \left(\frac{[O_2/Ar]_{sw}}{[O_2/Ar]_{eq}} - 1 \right) \times 100\% \quad (1)$$

In recent years, ship-based mass spectrometry has been employed to provide high-resolution coverage of NCP estimates from underway $\Delta O_2/Ar$ measurements (Kaiser et al., 2005; Tortell, 2005), yielding an improved understanding of the distribution of NCP (e.g., Kavanaugh et al., 2014; Eveleth et al., 2017; Juranek et al., 2019). However, the requirement for mass spectrometry generally limits deployments to research ships, while the expense of these instruments and the expertise required to deploy them at sea may be prohibitive to some research groups. Truly autonomous measurements on research vessels, volunteer observing ships (VOS), or *in-situ* platforms such as unmanned surface vehicles (USV) would significantly expand the global coverage of NCP estimates, helping to integrate these data with upper trophic level processes and observations of climatic variability across a range of scales.

Recent work has demonstrated that the seawater O_2/N_2 ratio, derived from simultaneous deployments of autonomous O_2

optode and gas tension device (GTD) sensors, may be used as an alternative to O_2/Ar measurements for high-resolution NCP estimates (Izett and Tortell, 2021). Observations from these instruments can be used to derive seawater nitrogen (N_2) concentrations (McNeil et al., 2005), and therefore calculate the biological O_2 saturation anomaly from *in-situ* O_2/N_2 measurements (i.e., $\Delta O_2/N_2$, following Eq. 1). Relative to $\Delta O_2/Ar$, however, $\Delta O_2/N_2$ does not fully account for physical impacts on O_2 , due to differences in the solubility properties of O_2 and N_2 .

Izett and Tortell (2021) described an approach to correct for physical offsets between $\Delta O_2/N_2$ and $\Delta O_2/Ar$, using readily available environmental data and a modeling framework. The approach yields a new tracer, $\Delta O_2/N_2'$ (denoted “ N_2 -prime”) which provides an analog for $\Delta O_2/Ar$. In principle, $\Delta O_2/N_2'$ holds significant promise as an NCP tracer under a range of oceanic conditions. To date, however, this approach has not been evaluated in the field, and no studies have reported NCP estimates derived from underway $\Delta O_2/N_2$ or $\Delta O_2/N_2'$. In this paper, we present an *in-situ* evaluation of $\Delta O_2/N_2$ and $\Delta O_2/N_2'$ as NCP tracers, using observations from three research cruises in the Subarctic Northeast Pacific and Canadian Arctic Ocean. Our measurements allow us to compare $\Delta O_2/N_2$, $\Delta O_2/N_2'$ and $\Delta O_2/Ar$ over broad spatial scales and contrasting hydrographic regimes, and to evaluate the accuracy of the associated O_2/N_2 -based NCP estimates. We demonstrate the strong utility of $\Delta O_2/N_2'$ as an alternative to $\Delta O_2/Ar$ for autonomous NCP measurements across a range of oceanic environments, while also identifying conditions where uncorrected $\Delta O_2/N_2$ is a useful NCP tracer. We evaluate potential errors in the estimation of NCP based on O_2/N_2 and provide recommendations for future deployments of optode/GTD systems as a tool for oceanic productivity measurements.

MATERIALS AND METHODS

Deployments

We present data from three research cruises conducted during 2018 and 2019; two in the Subarctic NE Pacific (September 2018 and February 2019; **Figure 1A**) and one in the eastern and central Canadian Arctic Ocean, spanning the Labrador Sea (LS), Baffin Bay (BB) and the Canadian Arctic Archipelago (CAA; July–August 2019; **Figure 1B**). We denote the datasets as “NEP-summer,” “NEP-winter” and “Arctic-summer.” The two Subarctic Northeast Pacific (NEP) expeditions were conducted on board the CCGS J. P. Tully, as part of the Line P monitoring program (Department of Fisheries and Oceans Canada, cruise IDs 2018-040 and 2019-001, respectively), while the Arctic deployment was conducted on the CCGS Amundsen, as part of the ArcticNet program (Leg 2, cruise ID 1902).

On all cruises, gas and hydrographic observations were obtained using an underway optode/GTD, membrane inlet mass spectrometer (MIMS) and thermosalinograph. Seawater was pumped from nominal intake depths of ~ 5 m (NEP cruises) and ~ 7.5 m (Arctic cruise) to the ship's laboratories and directed to the respective instruments. On the CCGS Tully, a progressive

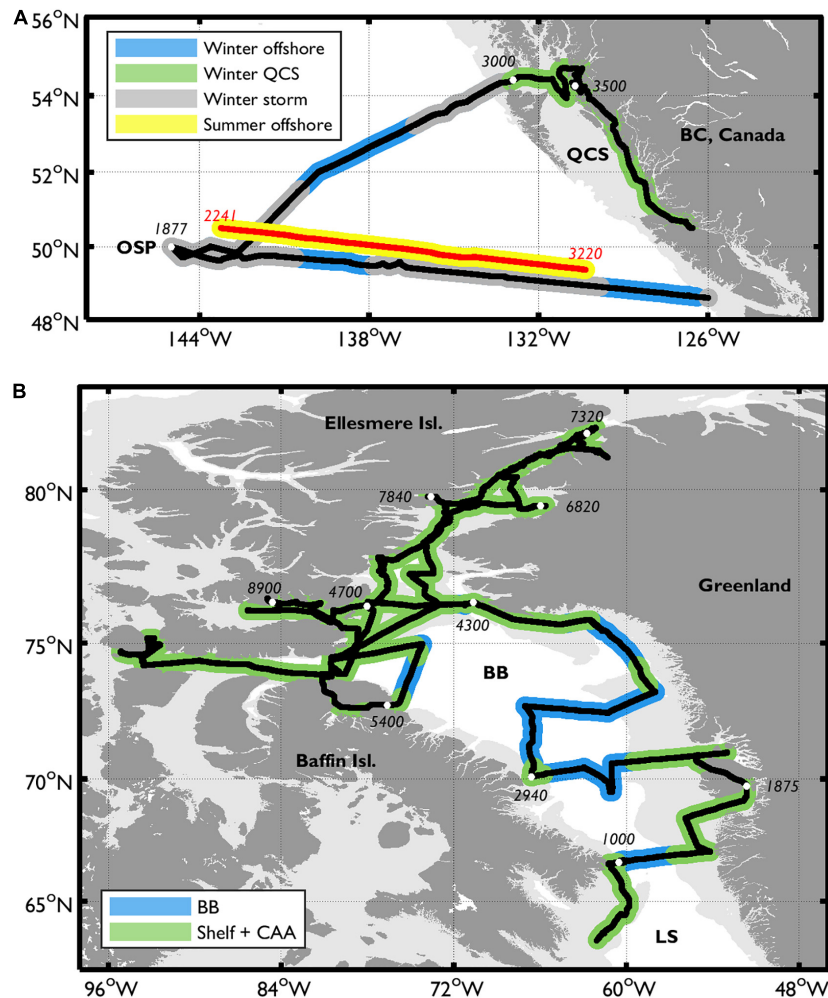


FIGURE 1 | Survey ship tracks in the Subarctic NE Pacific **(A)**, and the eastern Canadian Arctic **(B)** showing the locations where underway $\Delta O_2/Ar$ and $\Delta O_2/N_2$ were compared. The approximate along-track distance (in km) is indicated with white markers for reference. In **(A)**, black lines correspond with the NEP-winter track, while the red line represents the NEP-summer track, displaced north by 0.5-degrees for visibility. The thick gray lines in **(A)** represent regions that experienced elevated sea states and high surface winds. In both panels, pale gray shading represents the approximate continental shelf regions (<500 m bathymetry), and the sampling sub-regions are distinguished by color outlines around the cruise track lines. OSP, Ocean Station Papa; QCS, Queen Charlotte Sound; LS, Labrador Sea; BB, Baffin Bay; CAA, Canadian Arctic Archipelago.

cavity pump (Moyno, 3L8CDQ) was used to supply water from the ship's intake to the laboratory, while on the CCGS Amundsen, centrifugal magnetic drive pumps (thermosalinograph supply: March Pumps, BC-4C-MD; MIMS and optode/GTD laboratory: 1ST1H5A4-M01 NPE) were used. Pumped water was always obtained from within the mixed layer (**Supplementary Figure 3**). We omitted data corresponding with instances of instrument malfunction, and periods of seawater flow interruption resulting from ice blockages in the ship's pumping system.

Underway $\Delta O_2/Ar$ and $\Delta O_2/N_2$ Observations

Underway Gas Measurements and Data Processing

Measurements of O_2/Ar were made using a membrane inlet mass spectrometer (MIMS; Tortell, 2005). Briefly, seawater was

circulated at a constant flow rate and temperature through a cuvette equipped with a 0.18 mm thick silicone membrane interfaced to the vacuum inlet of the mass spectrometer. Measurements of the mass-to-charge ratios at 32 (O_2) and 40 (Ar) AMU were obtained at approximately 20 s intervals. Water from an air-equilibrated standard bottle was introduced into the MIMS system every 45–90 minutes by automatically switching the inflow water source between the direct seawater supply and standard bottle. The standard consisted of ~ 2 L of filtered seawater (<0.2 μm) gently bubbled using an aquarium air pump, and incubated at ambient sea surface temperature in an overflowing bucket. The seawater and air standard O_2/Ar ratios ($[O_2/Ar]_{sw}$ and $[O_2/Ar]_{eq}$, respectively) were used to derive underway $\Delta O_2/Ar$ (following Eq. 1) by linearly interpolating between air standard measurements. On the NEP-summer cruise, final underway $\Delta O_2/Ar$ was obtained by calibrating

the continuous measurements against discrete samples obtained from Rosette sampling (sample collection and processing details below). The underway data were linearly calibrated, with offsets between calibrated and uncalibrated signals ranging from $\sim 0\%$ (at $\Delta O_2/Ar$ values near equilibrium) to $\sim 3\%$ (at $\Delta O_2/Ar$ values of $\sim 10\%$). No calibrations were performed on the NEP-winter or Arctic datasets.

Underway O_2 and N_2 data were derived from seawater measurements obtained using a custom-built optode/GTD system (Izett and Tortell, 2020), as described in the following section. The system recorded O_2 concentration ($\mu\text{mol L}^{-1}$) and total dissolved gas pressure (i.e., the sum of all gas partial pressures; TP, mbar) at ~ 10 s intervals from an Aanderaa Data Instruments AS optode 4330 and Pro-Oceanus Systems Inc. mini-TDGP gas tension device, respectively. Debubbled seawater from the ship's supply line was pumped rapidly and at constant flow rate past the instruments ($\sim 2 \text{ L min}^{-1}$) to minimize the system residence time and hydrostatic pressure effects on the GTD measurements. A flow-through head (water residence time < 1 s) was installed on the face of the GTD to direct water onto the instrument's Teflon membrane. The optode was submerged in a 0.25 L flow-through cell (residence time < 10 s) and oriented so that water flowed onto the sensing foil.

To improve the alignment between the optode/GTD, MIMS and hydrographic data (described below), and account for the slower response time of the GTD relative to the other gas sensors, we filtered the underway data (O_2 , TP, $\Delta O_2/Ar$, temperature, salinity) before deriving $\Delta O_2/N_2$. All raw signals were low-pass filtered (frequency 0.5 min^{-1}) and subsequently median-binned into 2-min intervals. Following Hamme et al. (2015; their Eq. 2), we then applied a cumulative filter to all underway data (excluding GTD measurements) to replicate the rate of O_2 diffusion across the GTD membrane. We used a time-constant of $1/\tau_{\text{GTD}}$ (where τ_{GTD} is the GTD's temperature-dependent response time; $\sim 1\text{--}2$ min, Izett and Tortell, 2020), extrapolated to the ambient seawater temperature. Finally, we adjusted for time offsets between sensors by manually aligning measurement peaks. Unless stated otherwise, all data presented below were processed in this manner.

Calculation of $\Delta O_2/N_2$

Detailed handling and calibration procedures for O_2 , N_2 and $\Delta O_2/N_2$ are presented in the supporting material (Supplementary Material Section 1), and briefly summarized here. We corrected raw TP signals (TP^{cor}) for measurement bias (average offset < 1 mbar assessed as the difference between in-air GTD readings and atmospheric pressure) and for the effects of seawater warming between the intake and laboratory. Raw optode O_2 measurements were salinity-corrected (O_2^{cor}) following Uchida et al. (2008) and Bittig et al. (2018), and calibrated against discrete samples obtained from the outflow of the optode/GTD system or from Niskin bottles (details in the following section) to derive final O_2 concentrations (O_2^{cal}). Calibrated oxygen saturation ($O_{2,\text{sat}}^{\text{cal}}, \%$) was derived by dividing O_2^{cal} by the O_2 solubility (Garcia and Gordon, 1992, 1993) calculated using ambient sea level and water

vapor pressures (P_{SLP} and $P_{\text{H}_2\text{O}}$ obtained from reanalysis data products; see below) and sea surface salinity and temperature data from a thermosalinograph installed near the ship's intake

$$\left(\text{i.e. } O_{2,\text{sat}}^{\text{cal}} = \frac{O_2^{\text{cal}}}{O_{2,\text{eq}} \times \frac{P_{\text{SLP}} - P_{\text{H}_2\text{O}}}{1013.25 \text{ mbar} - P_{\text{H}_2\text{O}}}} \times 100\% \right).$$

We derived the N_2 partial pressure (pN_2) following McNeil et al. (2005) by subtracting the partial pressures of O_2 (obtained from $O_{2,\text{sat}}^{\text{cal}}$ following Eq. 2), Ar and water vapor from TP^{cor} measurements (Eq. S7). The Ar saturation state (Ar_{sat}) and partial pressure were estimated from MIMS $\Delta O_2/Ar$ and optode $O_{2,\text{sat}}^{\text{cal}}$ by re-arranging Eq. 1. The saturation state of all remaining gases (including Ar, when MIMS data were unavailable, and carbon dioxide) was assumed to be equivalent to N_2 , following McNeil et al. (2005). The N_2 saturation level ($N_{2,\text{sat}}$), and resulting $\Delta O_2/N_2$ (both %), were calculated following

$$N_{2,\text{sat}} = \frac{pN_2}{\chi N_2 \times (P_{\text{SLP}} - P_{\text{H}_2\text{O}})} \times 100\% \quad (2)$$

$$\Delta O_2/N_2 = \left(\frac{O_{2,\text{sat}}^{\text{cal}}}{N_{2,\text{sat}}} - 1 \right) \times 100\% \quad (3)$$

where χN_2 is the atmospheric dry mole fraction of N_2 (0.78084). As the saturation state of O_2 , Ar or N_2 is equal to the ratio of observed concentration and equilibrium concentration at ambient temperature, salinity and P_{SLP} , Eq. 1 (for $\Delta O_2/Ar$) and Eq. 3 (for $\Delta O_2/N_2$) are equivalent. Individual gas supersaturation states (ΔO_2 , ΔAr and ΔN_2) are calculated following the same convention as in Eq. 3 (i.e. $\Delta C = (C_{\text{sat}}/100 - 1) \times 100\%$). The equilibrium concentrations of N_2 and Ar were derived from the equations of Hamme and Emerson (2004) using temperature and salinity measurements made near the ship's intake.

Underway Signal Calibration and Discrete Gas Samples

On each cruise, optode measurements were calibrated against discrete samples obtained from the outlet of the optode/GTD system. Discrete samples were analyzed by Winkler titration (automated colorimetric and potentiometric endpoint determinations during the NEP and Arctic cruises, respectively). We derived a best-fit linear regression between calibration samples and corresponding optode measurements (averaged within 2 min of sampling), and adjusted the calibrated O_2 for concentration differences between samples obtained from the flow-through seawater supply and mixed layer Niskin bottles (Eq. 3). While we did not observe any evidence of O_2 consumption in the ships' seawater lines (Juraneck et al., 2010), calibrating the optode signal against discrete samples from surface Niskin bottle sampling should correct for such potential sampling artifacts in subsequent studies. Since optode sensitivity drifts during storage, and in some cases during deployments (D'Asaro and McNeil, 2013; Bittig et al., 2018), we performed calibrations using discrete samples obtained over a range of hydrographic conditions and O_2 concentrations throughout the duration of each deployment. A single linear calibration was derived for each separate cruise dataset.

During the NEP-summer and Arctic cruises, underway $N_{2,sat}$ data were calibrated using discrete gas samples obtained from Niskin bottles fired within the mixed layer as close to the depth of the seawater intake as possible. Discrete $N_{2,sat}$ was calculated using N_2/Ar ratios measured in the bottle samples and corresponding underway Ar_{sat} . We obtained broad coverage of discrete samples across the Arctic cruise track, but reduced coverage during NEP-summer, and no samples from NEP-winter. All samples were collected in a manner that avoided bubble contamination and were preserved with saturated mercuric chloride solution before analysis by mass spectrometry, following Emerson et al. (1999) (NEP-summer samples) and Kana et al. (1994) (Arctic samples). $\Delta O_2/Ar$ was also measured in the discrete NEP-summer samples for calibration of the underway MIMS data. While no calibrations of the underway $\Delta O_2/Ar$ data were performed on the NEP-winter or Arctic cruises, calibrations of $N_{2,sat}$ based on discrete N_2/Ar measurements and underway MIMS- and optode-derived Ar_{sat} should make the comparison of $\Delta O_2/Ar$ and $\Delta O_2/N_2$ intrinsically consistent.

Discrete gas samples for subsurface N_2/Ar analyses were also collected during the NEP-summer and Arctic cruises (Supplementary Figure 5). Samples were collected at various depths and analyzed as described above. Subsurface N_2/Ar data were used in calculating N_2' , as described below. Detailed discrete gas sampling and analysis procedures are presented in Supplementary Material Section 1.3.

In discussing our results, we present calibrated data and omit the “cal” and “cor” superscripts. Gases (O_2 , Ar or N_2) are represented by their saturation anomalies (i.e., $\Delta C = (C_{sat}/100 - 1) \times 100\%$) referenced at ambient P_{SLP} . We calculate offsets between $\Delta O_2/Ar$ and $\Delta O_2/N_2$ in two different ways: (1) based on their absolute difference (i.e., $\Delta O_2/Ar - \Delta O_2/N_2$); and (2) by using the tracer $\Delta N_2/Ar$ (calculated following Eq. 3 convention), which is independent of the O_2 saturation state. Gas ratios ($\Delta O_2/Ar$, $\Delta O_2/N_2$, and $\Delta N_2/Ar$) are not influenced by ambient P_{SLP} .

Ancillary Datasets

Continuous measurements of sea surface temperature (SST) and salinity were obtained from a thermosalinograph installed near the ships' seawater intakes (Sea-Bird SBE-21 and SBE-45/SBE-38 thermometer, on the CCGS Tully and CCGS Amundsen, respectively). Depth profiles of temperature and salinity were obtained from CTD casts (Sea-Bird SBE-911plus), and the mixed layer depth (MLD) was defined based on a 0.125 kg m^{-3} density difference from the mean value in the upper 5 m (Thomson and Fine, 2003). We performed a two-dimensional spatial interpolation of MLD between CTD stations to estimate the MLD along the entire cruise tracks. Hydrographic data were provided by the Institute of Ocean Sciences (Department of Fisheries and Oceans Canada)¹ and the Amundsen Science group of U. Laval (Amundsen Science Data Collection, 2020a,b).

We obtained wind speed data at 10-m elevation from the CCMPv2 vector (Atlas et al., 2011), and NARR reanalysis (Mesinger et al., 2006) products for the NEP and Arctic,

respectively. Gridded SST were from the NOAA High Resolution OI v2 dataset (Reynolds et al., 2007), and P_{SLP} and P_{H_2O} data from the NCEP/NCAR reanalysis products (Kalnay et al., 1996). Sea ice fractional coverage was obtained from the AMSR-2 product (Sprenn et al., 2008). The environmental data (excluding sea ice) were calibrated for our study regions using linear equations derived by comparing the gridded data with a multi-year ensemble of observations from moorings, buoys and ships in coastal and offshore waters (details in the **Supplementary Material**). The wind speed data were adjusted by $< 1.2 \text{ m s}^{-1}$, on average, across both regions, while SST and P_{SLP} gridded data were adjusted by $\sim 0.2^\circ\text{C}$ (NEP) and 0.6°C (Arctic) and 3 mbar, respectively. The average uncertainty in the adjusted wind speed, SST and SLP data, estimated as the mean deviation from ship-board measurements at the time of sampling was $\sim 3 \text{ m s}^{-1}$, 0.7°C and 2 mbar, respectively. We performed a nearest-neighbor interpolation of the adjusted gridded data to the cruise tracks at the time of data collection, and backward in time by 60 (NEP) to 90 (Arctic) days to determine the environmental histories of the sampling regions prior to the ship's arrival (Supplementary Figure 3). The interpolated data were used to perform N_2' calculations over the 60–90-day historical time period prior to our ship-based sampling. A longer (i.e., 90-day) time-record is required for ocean regions with longer mixed layer gas residence times.

N_2' : Correcting N_2 for Solubility, Bubble and Mixing Effects

Following Izett and Tortell (2021), we derived the term N_2' to reconcile physical differences in Ar and N_2 supersaturation (ΔAr and ΔN_2) resulting from differential solubility properties, air-sea exchange rates, bubble effects and vertical mixing and advection. Full details and evaluation of the model calculations are presented in the Izett and Tortell manuscript, while Matlab scripts with examples for performing N_2' calculations are available in a Matlab O2N2 NCP Toolbox² (Izett, 2021).

Briefly, we calculated the expected Ar and N_2 supersaturation difference ($\Delta N_2^{\text{mod}} - \Delta Ar^{\text{mod}}$) at the time of our measurements using a simple one-dimensional model forced with gridded environmental data over one O_2 re-equilibration timescale prior to the ship-board observations (T_{O_2} ; see below). The model evaluates the mixed layer (ML) evolution of gas C (N_2 or Ar) following:

$$\frac{d(C \times \text{MLD})}{dt} = F_d + F_C + F_P + \frac{C_{\text{deep}} - C}{dZ} \times k_Z \quad (4)$$

The first three terms on the right represent the air-to-sea flux via diffusive (F_d), and bubble-mediated ($F_C + F_P$; denoting fully collapsing and partially dissolving bubbles) processes, and the last term represents the vertical mixing flux. We used the model of Liang et al. (2013) to calculate the air-sea exchange terms in ice-free waters, and that of Butterworth and Miller (2016) to determine the total air-sea flux (F_C and F_P not explicitly parameterized) in partially ice-covered waters. The term $\frac{C_{\text{deep}} - C}{dZ}$

¹<http://www.waterproperties.ca/linep/>

²<https://doi.org/10.5281/zenodo.4024925>

(mmol m^{-4}) represents the vertical gradient of Ar or N_2 between the surface and a given depth below the mixed layer (dZ , equal to the thickness of the pycnocline, as described in Izett and Tortell, 2021; their Figure 1). The κ_Z term ($\text{m}^2 \text{d}^{-1}$) is the vertical mixing rate. Subsurface Ar (Ar_{deep}) was set to the equilibrium concentration at subsurface temperature and salinity conditions derived by interpolating CTD measurements along the cruise track, and $N_{2,\text{deep}}$ was derived from subsurface N_2/Ar data (i.e., $\Delta N_2/Ar_{\text{deep}}$) and Ar_{deep} . In the NEP-summer and Arctic cruises, $\Delta N_2/Ar_{\text{deep}}$ was measured from N_2/Ar samples (**Supplementary Figure 5** with further details in **Supplementary Material Section 1.3**), while archived data from Hamme et al. (2019) were used to characterize the deep gas conditions in NEP-winter (data provided at <https://doi.org/10.1575/1912/bco-dmo.744563>). κ_Z was derived from vertically resolved nitrous oxide (N_2O) measurements in the NEP (following Izett et al., 2018) and from NEMO circulation model simulations of the Arctic and N. Atlantic (NEMO model simulations described in Castro de la Guardia et al., 2019). In performing the N_2' calculations, we subdivided our survey regions into smaller zones, which are described below. Mean $\Delta N_2/Ar_{\text{deep}}$ and κ_Z values were applied in each of these sub-regions (**Supplementary Table 1**), except in the Arctic where we used along-track κ_Z values based on the NEMO model output. We evaluate the sensitivity of the N_2' calculations to these parameterizations in the discussion.

We calculated T_{O_2} , the O_2 re-equilibration time, as $-\ln(0.01) \times \text{MLD}/(k_T + \kappa_Z/dZ)$ (where k_T is the combined diffusive and large bubble-induced O_2 gas transfer velocity), and evaluated the budget by setting starting ML gas concentrations to C_{eq} . The re-equilibration timescale is approximately fivefold larger than the ML O_2 residence time ($\tau_{O_2} = \text{MLD}/k_T$; **Supplementary Figure 3**), in order to fully erase the initial conditions invoked in the N_2' model calculations. We assumed a constant MLD based on interpolated values from CTD casts. As discussed in Izett and Tortell (2021), this assumption may be problematic during periods of significant MLD changes (e.g., spring and autumn), but the uncertainty incurred in N_2' calculations remains small relative to other NCP errors. In each time step, we calculated C_{eq} from time-variable SST and P_{SLP} , and constant salinity (based on ship-board measurements). The modeled difference between Ar and N_2 supersaturation (ΔC^{mod}) at the time of our cruise observations was then subtracted from optode/GTD-derived ΔN_2 observations to obtain $\Delta N_2'$. We subsequently calculated $N_{2,\text{sat}}'$ from $\Delta N_2'$, and re-evaluated $\Delta O_2/N_2$ (as $\Delta O_2/N_2'$) following Eq. 3 convention.

$$\Delta N_2' = \Delta N_2^{\text{obs}} - (\Delta N_2^{\text{mod}} - \Delta Ar^{\text{mod}}) \quad (5)$$

Calculations of Net Community Production

We estimated NCP ($\text{mmol m}^{-2} \text{d}^{-1}$) as the product of the biological O_2 saturation anomaly, the O_2 equilibrium concentration (at 1013.25 mbar), and the O_2 gas transfer velocity (k_{O_2} , m d^{-1}).

$$\text{NCP} = k_{O_2} \times (\Delta O_2/C) \times [O_2]_{\text{eq}} \quad (6)$$

In this approach, C represents either Ar, N_2 or N_2' , and NCP is equivalent to the diffusive sea-air flux of biologically produced excess O_2 (Teeter et al., 2018). We used the diffusive gas transfer velocity parameterization from Liang et al. (2013) in the NEP, and that of Butterworth and Miller (2016) in the Arctic [i.e. k_{O_2} scaled to the fraction of ice-free water, f , as $k_{O_2} = k_{O_2} \times (1-f)$] to derive historical k_{O_2} values from the wind-speed observations. Final k_{O_2} was obtained by weighting these values over a 30-day period, following Teeter et al. (2018). Adjusting the length of the weighting period to account for different ML O_2 residence times does not have a significant effect on k_{O_2} . Examples of these calculations are provided in the O_2N_2 NCP toolbox at (see text footnote 2).

Below, we present NCP estimates calculated using the three different metrics of the biological O_2 saturation anomaly: $\Delta O_2/Ar$ -NCP, $\Delta O_2/N_2$ -NCP and $\Delta O_2/N_2'$ -NCP.

RESULTS

Our combined observations provide broad spatial coverage across a variety of oceanographic regimes throughout the Subarctic NEP and Canadian Arctic. In these contrasting regions, various physical and biological controls are expected to differentially affect gas saturation anomalies. For this reason, our combined dataset allowed us to examine a range of conditions under which measurements of $\Delta O_2/N_2$ or $\Delta O_2/N_2'$ can be used for accurate NCP derivation.

In describing our results, we divided the cruise tracks into distinct sub-regions (**Figure 1**). In the NEP, we differentiate between offshore (> 500 m water depth) and nearshore waters. We only present results from the offshore section of the return (eastward) transect of the NEP-summer cruise due to periodic instrument problems on the outbound leg. In the NEP winter cruise, sampling within the nearshore region occurred in the Queen Charlotte Sound (QCS; $> 2,700$ km along-track). In the Arctic, we identify nearshore waters as those occurring over the Baffin Bay continental shelf (all regions overlying the continental shelf $< 6,000$ km along-track; identified by light gray shading in **Figure 1B**) and in the Canadian Arctic Archipelago (CAA), and offshore waters of Baffin Bay (BB; excluding shelf regions $< 6,000$ km along-track).

Underway Signal Calibration

We observed a strong linear relationship between optode and Winkler-based O_2 concentrations ($R^2 = 0.99$ for each cruise), enabling calibration of the underway data with a root mean square error (RMSE) of $< 0.75\%$ (**Figure 2A**). The calibration samples were collected throughout the duration of each deployment over a wide range of hydrographic conditions and O_2 concentrations (bars in **Figure 2A**), such that the calibrated O_2 should be accurate for the conditions encountered on each cruise.

We also observed a strong linear relationship between underway and discrete $N_{2,\text{sat}}$ ($R^2 = 0.90$, $\text{RMSE} = 0.90\%$ in the pooled NEP-summer and Arctic dataset; **Figure 2B**). Given the accuracy of O_2 (calibrated to $< 1\%$) and TP ($\pm 0.1\%$, per Pro-Oceanus Systems Inc.) measurements, this calibration validates

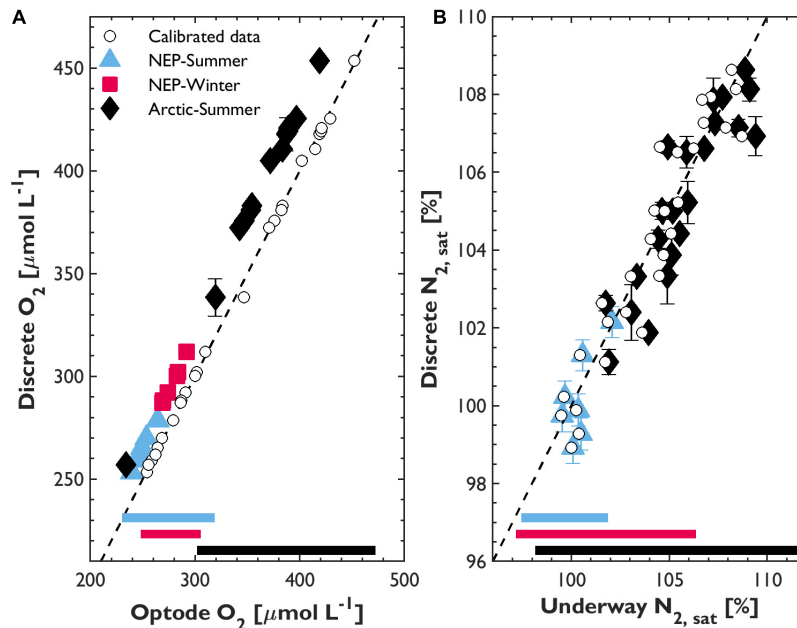


FIGURE 2 | Calibration of underway O_2 (A) and $N_{2,sat}$ (B) against discrete samples obtained from 2018 and 2019 Line P and Arctic cruises. Discrete O_2 samples were obtained from the seawater supply line, while N_2 samples were taken from Niskin bottles closed in the mixed layer. Underway sensor data (x-axis) represent the mean signal during a 2-min interval around the time of discrete sample collection. Error bars represent one standard deviation of the mean of duplicate discrete data; the standard deviation of the underway data is too small to resolve on the figure. The dashed line is the 1:1 line, and the bars at the bottom of each panel show the range of observed underway O_2 and N_2 on each cruise, excluding data during storm-impacted segments. The lowest Arctic O_2 calibration point (black diamond $\sim 260 \mu\text{mol L}^{-1}$) represents an air-equilibrated standard obtained by bubbling seawater at $\sim 18^\circ\text{C}$ before manually circulating through the optode/GTD system at the end of the Arctic cruise.

the underway $N_{2,sat}$ data within an accuracy of $\sim 1\%$. Moreover, as discrete N_2 was derived using N_2/Ar ratios measured in the bottle samples and MIMS-based Ar_{sat} , this result suggests a similar accuracy for the underway $\Delta O_2/\text{Ar}$ data.

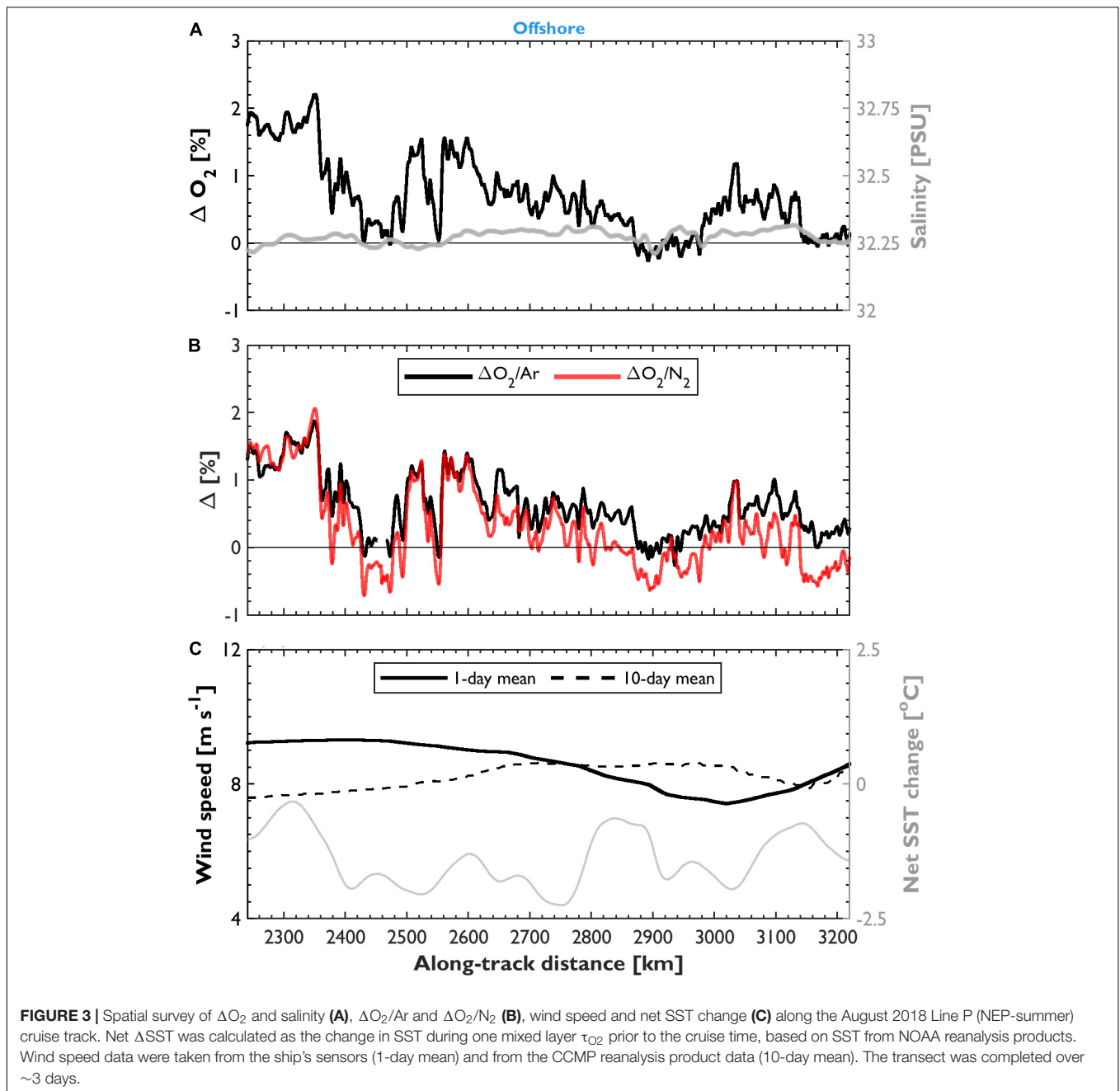
Since the NEP-summer and winter deployments used the same gas sensors, and we observed no drift in the GTD measurements over time (i.e., constant offset against atmospheric pressure), we applied the NEP-summer N_2 calibration to both datasets. Although the range of TP and $N_{2,sat}$ conditions we encountered differed between the cruises (bars in **Figure 2B**), calibrations based on the NEP-summer, Arctic or pooled datasets resulted in derived $\Delta O_2/N_2$ that varied by less than 0.4%. Across all cruises, the maximum difference between calibrated and uncalibrated $N_{2,sat}$ was $\sim 2\%$ at the highest saturation levels (mean $\sim 0.2\%$), suggesting that biases in $\Delta O_2/N_2$ and derived NCP should be small even without N_2 calibrations. However, as the calculation of $N_{2,sat}$ is sensitive to the degree of seawater warming between the ship's intake and GTD (details in **Supplementary Material Sections 2, 4**), TP measurements should be made as close as possible to the ship's seawater intake to minimize this source of error when calibration is not possible.

Surface Water Hydrography, Physical Forcing, and Gas Saturation Anomalies

We observed substantial spatial variability in surface hydrography (represented by sea surface salinity) across

the study regions, and large temporal variability in physical forcing (wind speed, temperature changes and sea ice cover) prior to the cruise measurements. These factors contributed to large variations in mixed layer gas saturation states ($\Delta O_2/\text{Ar}$, $\Delta O_2/N_2$, ΔO_2 , ΔAr , and ΔN_2). **Figures 3–5** summarize underway observations as well as wind speed and SST change (ΔSST) over the mixed layer residence time of O_2 , τ_{O_2} . **Supplementary Figures 2, 3** present the along-track ΔN_2 and ΔAr observations and environmental histories, respectively.

Prior to our observations, wind speed and SST were highly variable in the NEP and Arctic, while Arctic sea ice coverage showed a declining trend (**Supplementary Figure 3**). On average, wind speeds during and prior to the NEP-winter cruise were higher and more variable than during the summer cruises (**Figures 3C, 4C, 5C** and **Supplementary Figure 3**). Several high-wind events (wind speed $> 10 \text{ m s}^{-1}$) occurred near the time of our winter sampling, while wind speeds during and in the 60-days prior to the summer deployments were mostly below 10 m s^{-1} . Throughout most of the NEP-winter transect, surface waters experienced net cooling before the cruise, with the greatest cooling ($\sim 3^\circ\text{C}$ over τ_{O_2}) observed in nearshore waters. The summertime NEP cruise also experienced net cooling of around 2°C over τ_{O_2} . In contrast, warming was recorded over nearly the entire Arctic cruise track (ΔSST range -2 – 7°C ; **Figure 5C**), with cooling observed in only several isolated regions.



Gas Observations in the Subarctic Northeast Pacific

Gas distributions and hydrographic properties differed between the summer and winter NEP cruises (**Figures 3, 4** and **Supplementary Figures 2, 3**). Along the offshore NEP-summer track, we generally observed little spatial variability in all gases and hydrographic properties (**Figure 3**). During this summer cruise, ΔO_2 , ΔAr and ΔN_2 were all within $\sim 2\%$ of saturation, and $\Delta O_2/Ar$ and $\Delta O_2/N_2$ strongly mirrored patterns in ΔO_2 . $\Delta O_2/Ar$ typically exceeded $\Delta O_2/N_2$ (i.e., $\Delta N_2 > \Delta Ar$), and values ranged from ~ -0.75 to 2% .

During NEP-winter, we observed extremely high ΔO_2 , ΔAr and ΔN_2 (up to ~ 40 – 50% ; **Figure 4A** and **Supplementary Figure 2B**) corresponding with periods of very rough sea states and elevated wind speeds in offshore waters (blue shaded areas in **Figure 4**). In these stormy regions, $\Delta O_2/N_2$ was highly erratic and exhibited some extremely low values (minimum -18% ; **Figure 4B**), while $\Delta O_2/Ar$ showed little variability. Throughout the remainder of the winter transect, ΔO_2 was mostly undersaturated, and ΔAr and ΔN_2 were nearer to saturation ($\pm 5\%$). $\Delta O_2/Ar$ almost always exceeded $\Delta O_2/N_2$,

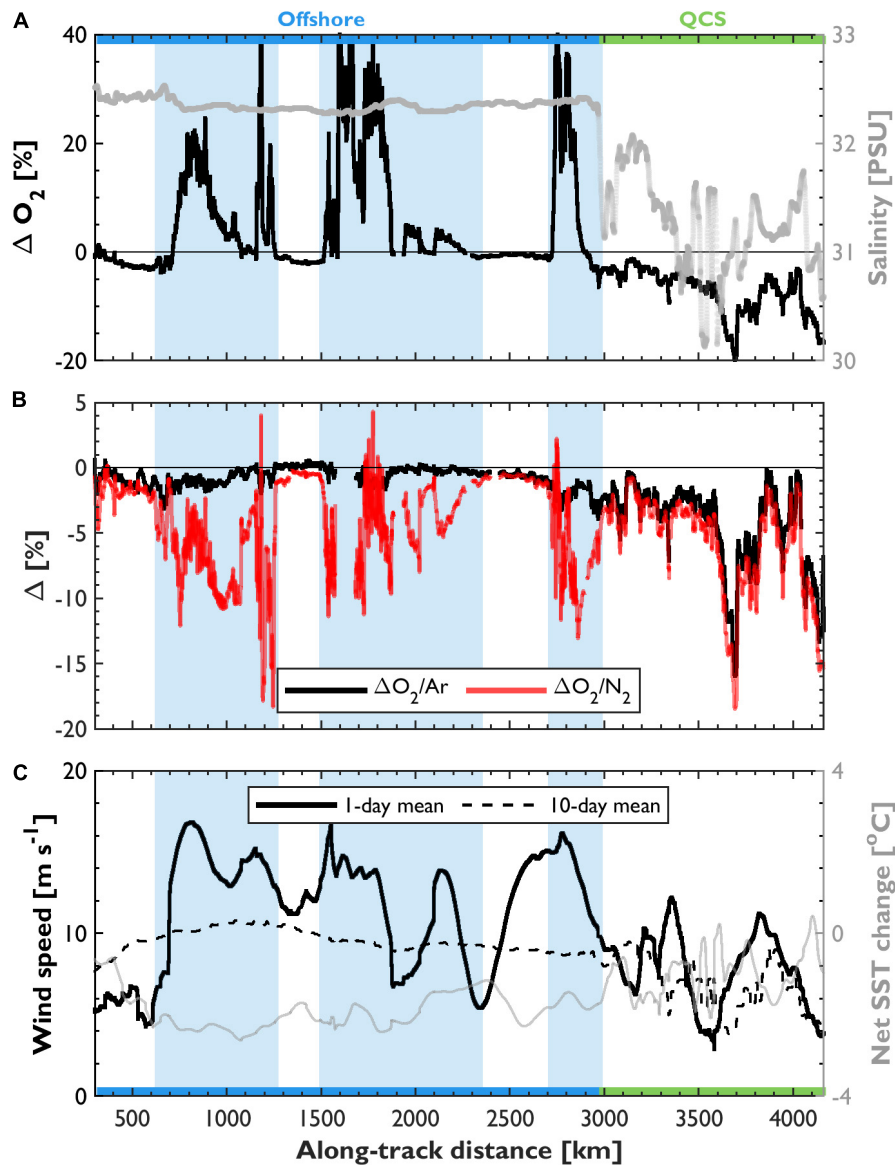


FIGURE 4 | Spatial survey of ΔO_2 and salinity **(A)**, $\Delta O_2/Ar$ and $\Delta O_2/N_2$ **(B)**, wind speed and net SST change **(C)** along the February 2019 Line P (NEP-winter) cruise track. The vertical light blue bars identify stormy sections of the transect. As described in the text, data from these regions were excluded from our analyses. The locations of the offshore and QCS regions are indicated by colored bars in **(A,C)**, corresponding with those in **Figure 1**. The transect was completed over ~ 15 days. Refer to **Figure 3** caption for further details.

and both tracers had an overall range of ~ -20 – 2% , strongly reflecting ΔO_2 variability. The lowest and most variable ΔO_2 values occurred in the nearshore QCS archipelago, corresponding with strong hydrographic fronts (**Figure 4A**). The largest offset between $\Delta O_2/Ar$ and $\Delta O_2/N_2$ also occurred in the QCS region, where ΔN_2 was up to $\sim 2.5\%$ higher than ΔAr .

Gas Observations in the Canadian Arctic

Gas saturation anomalies during the Arctic cruise contrasted those observed in the NEP (**Figures 5A,B**). Most notably, all gases (O_2 , Ar , and N_2) were supersaturated and highly variable along most of the transect. $\Delta O_2/Ar$ typically exceeded

$\Delta O_2/N_2$ ($\Delta N_2 > \Delta Ar$), and both were typically positive. As in the NEP, the distributions of $\Delta O_2/Ar$ and $\Delta O_2/N_2$ followed patterns in ΔO_2 , with the highest values (~ 10 – 30%) occurring in the shelf and CAA regions ($\sim 2,000$ and $> 6,000$ km along-track). Additional variability in ΔO_2 , $\Delta O_2/Ar$, and $\Delta O_2/N_2$ corresponded with significant salinity features in the vicinity of freshwater sources from glacier run-off and river discharge throughout the shelf and CAA (e.g., sharp drops in salinity $\sim 5,400$, $6,400$, $6,800$, $7,800$, and $8,800$ km; **Figure 5A**). ΔAr and ΔN_2 (**Supplementary Figure 2C**) were also higher and more variable in the Arctic than in the NEP (excluding storm-affected regions).

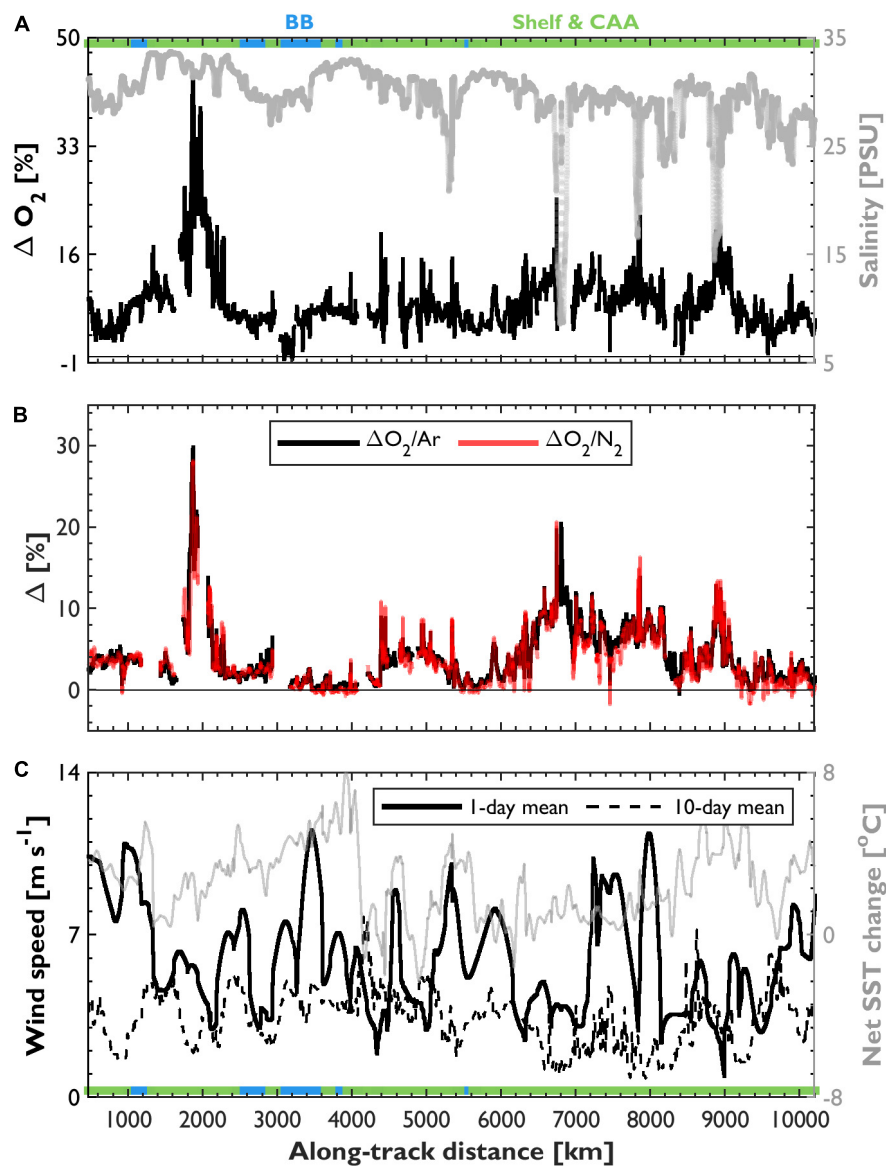


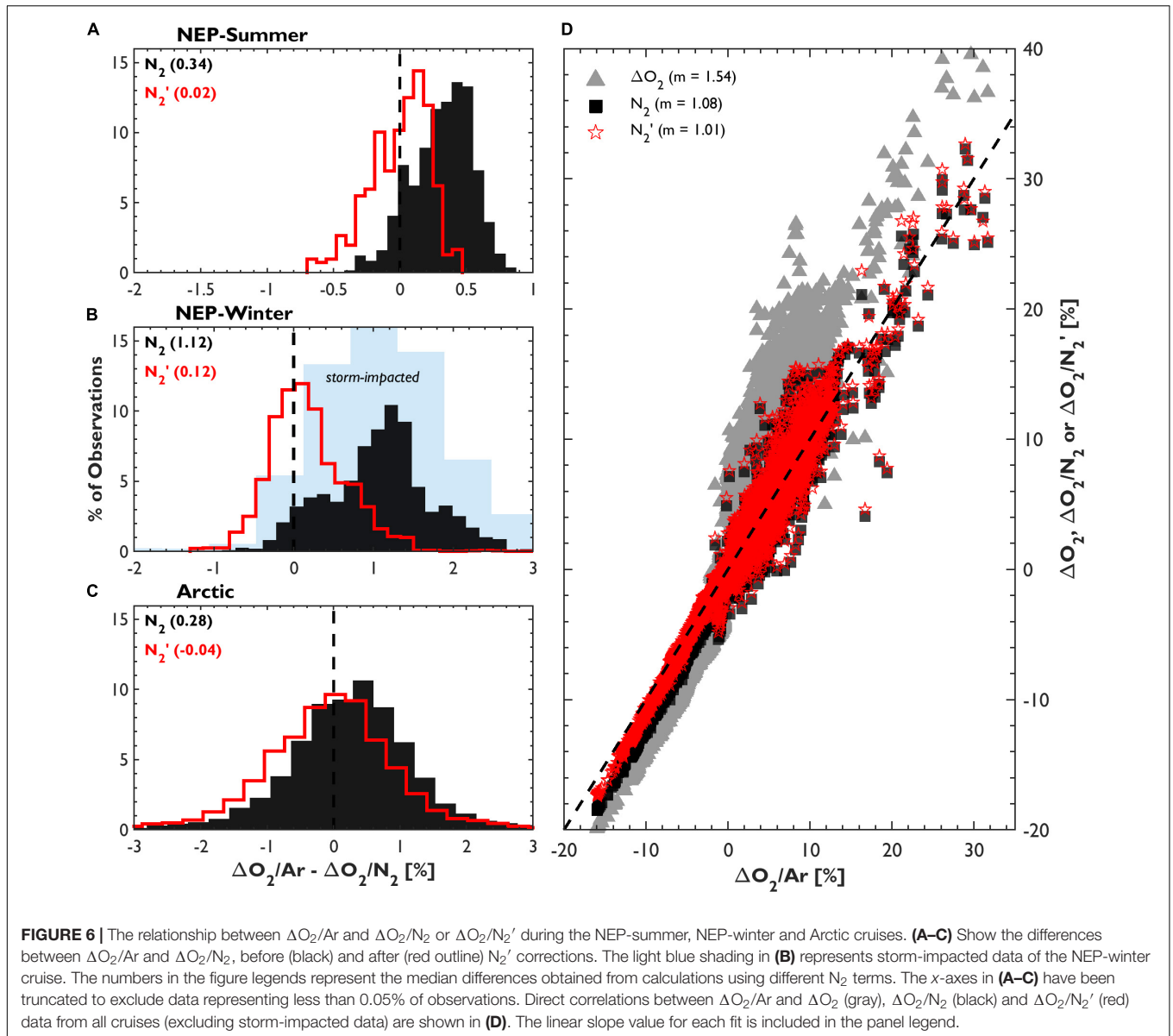
FIGURE 5 | Spatial survey of ΔO_2 and salinity (A), $\Delta O_2/Ar$ and $\Delta O_2/N_2$ (B), wind speed (NARR database) and net SST change (C) along the summer 2019 CCGS Amundsen (Arctic-summer) cruise track. The locations of the different regions are indicated by colored bars in (A,C). The transect was completed over ~ 40 days. Refer to **Figure 3** caption for further details.

Comparison of Underway $\Delta O_2/Ar$, $\Delta O_2/N_2$, and $\Delta O_2/N_2'$

The distribution of $\Delta O_2/Ar$ and $\Delta O_2/N_2$ (excluding the storm-impacted sections of the NEP-winter) exhibited high spatial coherence on all cruises (**Figures 3B, 4B, 5B, 6**). The linear slope of the $\Delta O_2/Ar$ vs. $\Delta O_2/N_2$ relationship was 1.08 ± 0.04 ($R^2 = 0.96$; uncertainty represents one-95% confidence interval around the least-squares slope) for the pooled dataset. These results demonstrate, to first order, the potential to use $\Delta O_2/N_2$ as an NCP tracer in place of $\Delta O_2/Ar$. In addition, $\Delta O_2/N_2$ showed greater spatial coherence with $\Delta O_2/Ar$ than ΔO_2 alone (pooled dataset slope = 1.54 ± 0.03), supporting the

continued normalization of O_2 measurements by a gas analog for NCP derivation.

Despite the good agreement between $\Delta O_2/Ar$ and $\Delta O_2/N_2$, small differences between the tracers remain. **Figures 6A–C** and **Supplementary Figure 4** show the cruise-wide and regional offsets between $\Delta O_2/Ar$ and $\Delta O_2/N_2$ before and after applying the N_2' calculations. We observed median differences between $\Delta O_2/Ar$ and $\Delta O_2/N_2$ of 0.3, 1.1, and 0.3% in the NEP-summer, -winter and Arctic datasets, respectively. Maximum deviations were up to $\sim 12\%$ (excluding storm-impacted data with wind speeds exceeding $\sim 10 \text{ m s}^{-1}$), and the range of values was $\sim 18\%$. As discussed below, the most extreme values likely represent



sampling artifacts rather than true differences between ΔAr and ΔN_2 .

Applying the N_2' corrections increased the alignment with $\Delta\text{O}_2/\text{Ar}$ on regional and sub-regional scales. Median offsets between $\Delta\text{O}_2/\text{Ar}$ and $\Delta\text{O}_2/\text{N}_2'$ were reduced to approximately 0.02% (NEP-summer), 0.1% (NEP-winter) and -0.04% (Arctic). The largest reduction in the bias between tracers occurred during the winter NEP cruise, while throughout the Arctic, $\Delta\text{O}_2/\text{N}_2$ and $\Delta\text{O}_2/\text{N}_2'$ were more similar. Overall, the direct comparison between all pooled $\Delta\text{O}_2/\text{Ar}$ and $\Delta\text{O}_2/\text{N}_2'$ observations had a linear regression slope not significantly different from unity (1.01 ± 0.03 with R^2 of 0.96).

Net Community Production Estimates

We did not compare $\Delta\text{O}_2/\text{Ar}$ -, $\Delta\text{O}_2/\text{N}_2$ -, and $\Delta\text{O}_2/\text{N}_2'$ -based NCP values on a point-by-point basis, since results are influenced

by the differential response times of the gas sensors. Rather, we compared NCP estimates after binning the respective datasets into 20-km intervals. **Table 1** and **Figure 7** summarize the derived NCP values by sub-region.

We observed the largest range of NCP values in the nearshore (QCS) waters of the Subarctic NE Pacific, and highest values (up to $\sim 30 \text{ mmol O}_2 \text{ m}^{-2} \text{ d}^{-1}$) in the Arctic shelf and CAA. Derived values were mostly negative during NEP-winter, and predominantly positive in both summer cruises. The strong negative values in the QCS likely reflect biases from vertical mixing of low O_2 waters, rather than *in situ* heterotrophy. Whereas NCP estimates derived from uncorrected $\Delta\text{O}_2/\text{N}_2$ showed a higher frequency of negative values compared with $\Delta\text{O}_2/\text{Ar}$ -derived NCP (15% of pooled dataset), application of N_2' significantly reduced the frequency of negative values (to 4%) in all sub-regions. Our observations thus suggest

that NCP estimated from $\Delta O_2/Ar$ and $\Delta O_2/N_2'$ provided consistent representation of the metabolic state of surface waters on regional scales. Moreover, as shown in **Figure 7B**, N_2' calculations reduced biases in derived NCP across the dataset. Indeed, $\Delta O_2/N_2'$ -NCP values calculated in each sub-region were generally closer to $\Delta O_2/Ar$ -based estimates, with median offsets $< 2 \text{ mmol O}_2 \text{ m}^{-2} \text{ d}^{-1}$, as compared to $< 9 \text{ mmol O}_2 \text{ m}^{-2} \text{ d}^{-1}$ for $\Delta O_2/N_2$ -NCP. In contrast to the NEP cruises, however, NCP estimates derived $\Delta O_2/N_2'$ and $\Delta O_2/N_2$ were nearly equivalent in parts of the Arctic (particularly in shelf and CAA waters), suggesting that N_2' was less important for reducing NCP biases in this region during the time of our sampling.

DISCUSSION

Uncertainty and Artifacts in Surface $\Delta O_2/N_2$ Observations

A key result of this work is that $\Delta O_2/Ar$ and $\Delta O_2/N_2$ show strong spatial coherence across all cruise transects, excluding regions in the Subarctic Pacific impacted by winter storms. Despite this overall agreement, important differences exist between these measurements, leading to $\Delta N_2/Ar$ disequilibria and offsets in derived NCP estimates. These can be attributed to physical processes, including solubility changes and bubble and mixing effects, which cause ΔAr and ΔN_2 to diverge, and to analytical or measurement uncertainty which must also be considered.

Bubble Entrainment During Elevated Sea States

The anomalous gas observations in parts of the offshore Subarctic NE Pacific winter data represent a limitation of the present application of O_2/N_2 -based NCP estimates. Several lines of evidence suggest that the exceedingly high ΔO_2 , ΔAr , and ΔN_2 and strongly negative $\Delta O_2/N_2$ measured in the wintertime offshore Subarctic NEP (**Figures 4A,B** and **Supplementary Figure 2B**) reflect artifacts from bubble entrainment in the ship's seawater supply during periods of elevated sea states. Following Vagle et al. (2010), application of the ideal gas law ($n = (f \times \chi \times p_{SLP}) / (R \times SST)$) shows that dissolution of bubbles with an air-volume fraction (f) of only $\sim 4\%$ is sufficient to yield the elevated ΔO_2 , ΔAr , and ΔN_2 values observed during the cruise (up to $\sim 45\%$). In contrast, observed noble gas and N_2 supersaturation seldom exceed $\sim 6\%$ in the subarctic ocean (Steiner et al., 2007; Emerson and Bushinsky, 2016; Hamme et al., 2019), even under extreme hurricane-force winds (wind speeds up to 57 m s^{-1} ; D'Asaro and McNeil, 2008). Moreover, most air-sea exchange parameterizations predict bubble-induced supersaturation anomalies of O_2 , N_2 , and Ar of less than $\sim 6\%$ at wind speeds below 20 m s^{-1} . Only extremely rapid warming ($> 10^\circ\text{C}$ over several days) could yield such strong positive supersaturation anomalies of all three gases, but we observed net cooling before the winter cruise (**Figure 4C**). Finally, such anomalies do not reflect sampling artifacts in the optode/GTD system, since it was designed to successfully divert bubbles from the instrument interfaces (Izett and Tortell, 2020). We thus conclude that the anomalously high gas supersaturation values we observed during the NEP-winter cruise resulted from bubble

dissolution in the $\sim 100 \text{ m}$ of piping between the ship's seawater intake and laboratory.

As O_2 and Ar have very similar solubility properties, the bubble effect on $\Delta O_2/Ar$ is small (but not entirely negligible for high rates of bubble dissolution). In contrast, the reduced solubility of N_2 relative to O_2 results in elevated N_2 sensitivity to bubble dissolution and a large negative $\Delta O_2/N_2$ anomaly. Based on these observations, we suggest that O_2/N_2 measurements should not be used to calculate NCP when significant bubble dissolution in the ship's underway sampling system is suspected. More generally, the set of criteria we used to discard $\Delta O_2/N_2$ data (i.e., strongly negative $\Delta O_2/N_2$ corresponding with $\Delta N_2 > \Delta O_2$ and both $> \sim 5\%$) should be applicable to many ocean regions that experience modest short-term temperature changes and minimal microbial N_2 production. Future work should, however, evaluate our criteria for other ships and ocean regions. For example, it is important to note that negative $\Delta O_2/N_2$ does not imply poor data quality, *per se*. The nearshore waters of the NEP-winter cruise provide an example of negative $\Delta O_2/N_2$ (**Figure 4B**) likely resulting from significant vertical fluxes of O_2 -deplete water, rather than bubble entrainment artifacts. Observations should thus be considered in light of the environmental forcing histories prior to sampling, and of additional gas fluxes that may produce negative $\Delta O_2/N_2$. Moreover, we note that elevated wind speeds alone may not be a strong criterion for identifying potentially biased data, since we encountered periodic u_{10} exceeding 10 m s^{-1} without excursions in the gas data during the Arctic cruise (**Figure 5**). Finally, our data quality criteria may not identify impacts of smaller bubble dissolution signatures, but such effects could be diagnosed by careful inspection of the underway data for differences in stochastic N_2 variability relative to O_2 . Indeed, as the underway sampling suggests, the spatial and temporal variability of O_2 is typically much greater than that of N_2 or Ar (compare ΔO_2 in **Figures 3A, 4A, 5A** with ΔAr and ΔN_2 in **Supplementary Figure 2**). Overall, bubble artifacts can likely be reduced by installing the optode/GTD system closer to the seawater intake, thereby reducing the distance and time over which bubbles can dissolve. This issue should also be less important on larger ships which are less susceptible to rolling and pitching during elevated sea states, or on ships with deeper intakes where the chance of entraining air in the underway seawater system is reduced.

Additional Sources of Analytical Uncertainty

Outside of the storm-impacted sections, we observed median offsets between $\Delta O_2/Ar$ and $\Delta O_2/N_2$ of less than $\sim 1.5\%$ in all cruise regions. Given the calibrated accuracy of the underway O_2 , $N_{2,sat}$ and $\Delta O_2/Ar$ data, we believe that these median signals largely represent real physical differences between $\Delta O_2/Ar$ and $\Delta O_2/N_2$. However, the full range of differences between $\Delta O_2/Ar$ and $\Delta O_2/N_2$ extended from ~ -6 to 12% . This large range is attributable to some sources of measurement uncertainty and the sensitivity of N_2 calculations to various assumptions, which contribute to a mean uncertainty in $\Delta O_2/N_2$ of $\sim 1.3\%$ (details in **Supplementary Material Section 2.4**). By comparison, the absolute uncertainty in underway $\Delta O_2/Ar$ is $\sim 0.75\%$, and the combined error in $\Delta O_2/Ar - \Delta O_2/N_2$ is $\sim 1.5\%$.

TABLE 1 | Summary of NCP estimates, differences between NCP terms and other biases in NCP calculations during the 2018 and 2019 NEP-summer, NEP-winter and Arctic cruises.

Cruise:		NEP-summer	NEP-winter		Arctic	
Region:		Offshore	Offshore	QCS	BB	Shelf and CAA
NCP	O_2/Ar	4.8 ± 3.5	-4.4 ± 5.1	-24.5 ± 12.0	2.0 ± 1.4	6.5 ± 6.4
	O_2/N_2'	4.2 ± 4.8	-6.4 ± 4.8	-24.8 ± 13.8	2.6 ± 2.0	6.6 ± 7.2
NCP difference (% opposite sign)	O_2/N_2	1.7 ± 4.8	-8.7 ± 5.3	-32.7 ± 12.8	1.6 ± 2.1	5.9 ± 6.8
	$O_2/Ar - O_2/N_2'$	1.1 ± 1.0 (10)	2.0 ± 2.5 (2)	1.9 ± 1.7 (0)	0.6 ± 0.9 (5)	0.8 ± 2.1 (3)
	$O_2/Ar - O_2/N_2$	3.0 ± 1.4 (30)	4.1 ± 3.6 (5)	8.9 ± 2.2 (0)	0.8 ± 0.7 (0)	1.1 ± 1.9 (1)
	Mixing bias	4.8 ± 2.3	8.4 ± 3.2	92.9	5.8 ± 6.2	6.3 ± 12.1
	Error due to k_{O_2} uncertainty	1.5 ± 1.0	1.7 ± 1.4	6.7 ± 3.3	0.7 ± 0.4	2.5 ± 2.0

Numbers represent median values (\pm one standard deviation) with units of $mmol O_2 m^{-2} d^{-1}$. Values in parentheses ("NCP difference" row) represent the percent of NCP observations that have opposite signs (e.g., $\Delta O_2/Ar-NCP > 0$ corresponding with $\Delta O_2/N_2-NCP < 0$). The O_2 mixing bias was estimated from N_2O and O_2 measurements (Izett et al., 2018) in the NEP cruises, and from κ_Z and O_2 profiles obtained from NEMO model simulations and CTD profiles in the Arctic. The NCP error due to ~ 20 – 40% uncertainty in the O_2 gas transfer velocity term (k_{O_2}) represents mean values in each sampling region based on $\Delta O_2/Ar-NCP$.

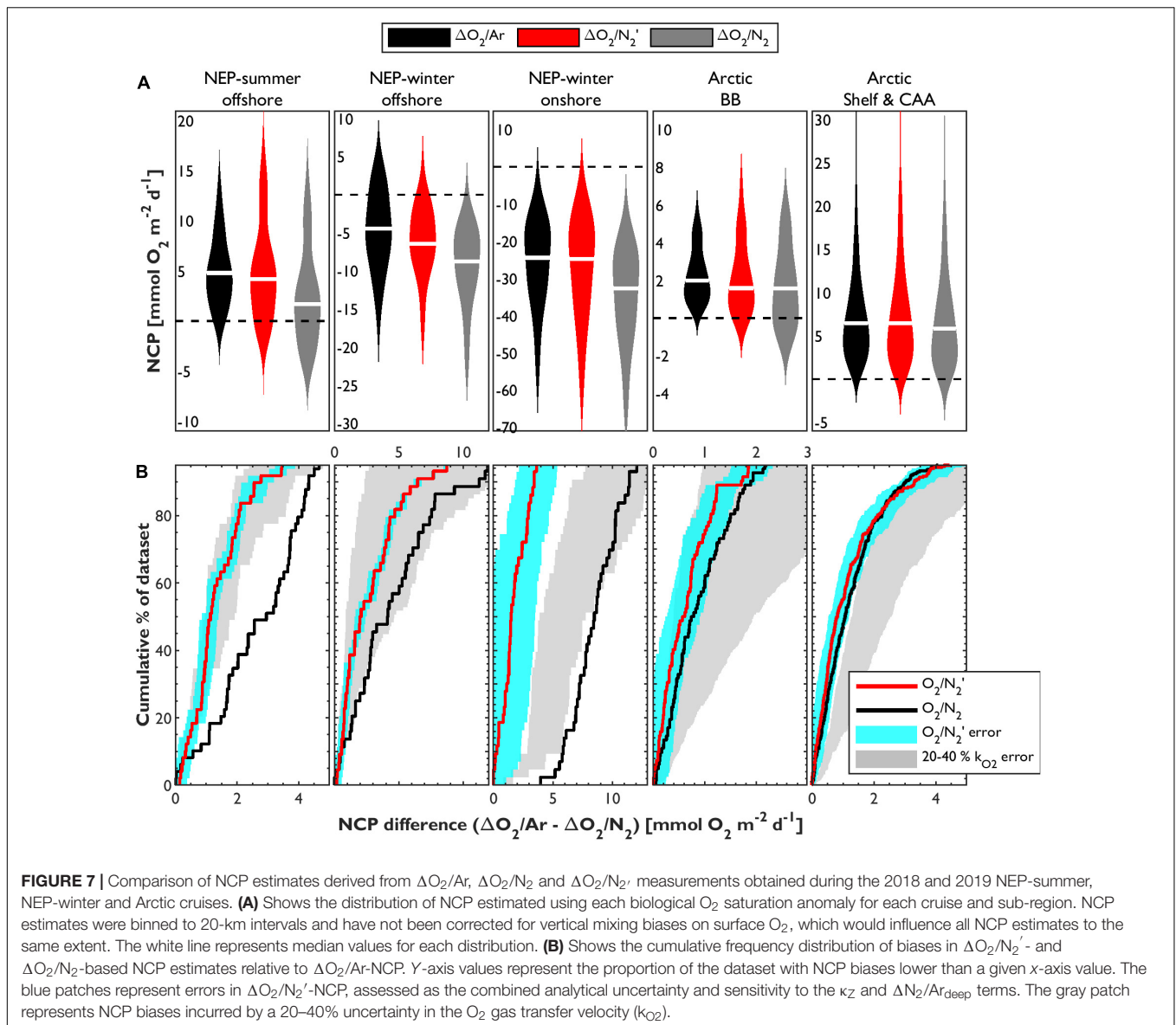
More extreme biases between $\Delta O_2/Ar$ and $\Delta O_2/N_2$ are attributed to other sampling artifacts, resulting from differences in the response times of the respective gas sensors. Although our data were filtered to the response time of the GTD (the slowest sensor) and adjusted for signal offsets before performing subsequent calculations, considerable transient biases between $\Delta O_2/Ar$ and $\Delta O_2/N_2$ remain when comparing individual data points. These offsets were most noticeable in waters with strong hydrographic gradients (e.g., near land masses and glacial regions), as demonstrated in **Figure 8**, which shows a subsection of the Arctic transect through a coastal fjord ($\sim 8,800$ km in **Figures 1, 5**). Although there is clear coherence between $\Delta O_2/Ar$ and $\Delta O_2/N_2$ (**Figure 8B**), the slow GTD response produces transient differences between $\Delta O_2/Ar$ and $\Delta O_2/N_2$ around hydrographic fronts. This problem, which is more significant in the unfiltered data, manifests as a large range in $\Delta O_2/Ar - \Delta O_2/N_2$ and extended tails in **Figures 6A–C**. The smoothing we applied reduces these transient signals but does not eliminate them altogether. Additional smoothing and filtering of the data may reduce such offsets, but the spatial features of the resulting datasets would be significantly dampened. Outside of strong frontal regions, or where $\Delta O_2/Ar$ and $\Delta O_2/N_2$ are low, this issue is less significant.

In future studies of $\Delta O_2/N_2-NCP$, we recommend the data processing procedures outlined above. Additional data treatment may be required to selectively remove signals clearly impacted by the slower response of the GTD relative to the optode. This procedure could, for example, be facilitated by comparing $\Delta O_2/N_2$ and SST signals. The O_2/N_2 measurement system used in this study was designed to optimize GTD response times (Izett and Tortell, 2020), so the issues described here reflect current instrumentation limitations and are unavoidable without further data filtering. Overall, this problem, while not insurmountable, should motivate continued development of GTD technology with more rapid response times.

Explaining Differences Between $\Delta O_2/Ar$ and $\Delta O_2/N_2$

Izett and Tortell (2021) recently developed a one-dimensional model to evaluate the contributions of various physical processes to divergence between $\Delta O_2/Ar$ and $\Delta O_2/N_2$ (i.e., $\Delta N_2/Ar$ disequilibrium) in the Subarctic NE Pacific. These simulations demonstrated the coupling between seasonal SST trends and $\Delta N_2/Ar$ variability in temperate waters. Rapid SST changes and short-term elevated wind events or SLP variability were shown to induce more transient responses, while combined bubble and vertical mixing fluxes contributed to seasonal alterations in baseline $\Delta N_2/Ar$, leading to higher winter values. As we discuss below, our field observations are consistent with these results, and with surface inert gas observations reported elsewhere (Hamme and Emerson, 2006; Hamme et al., 2017).

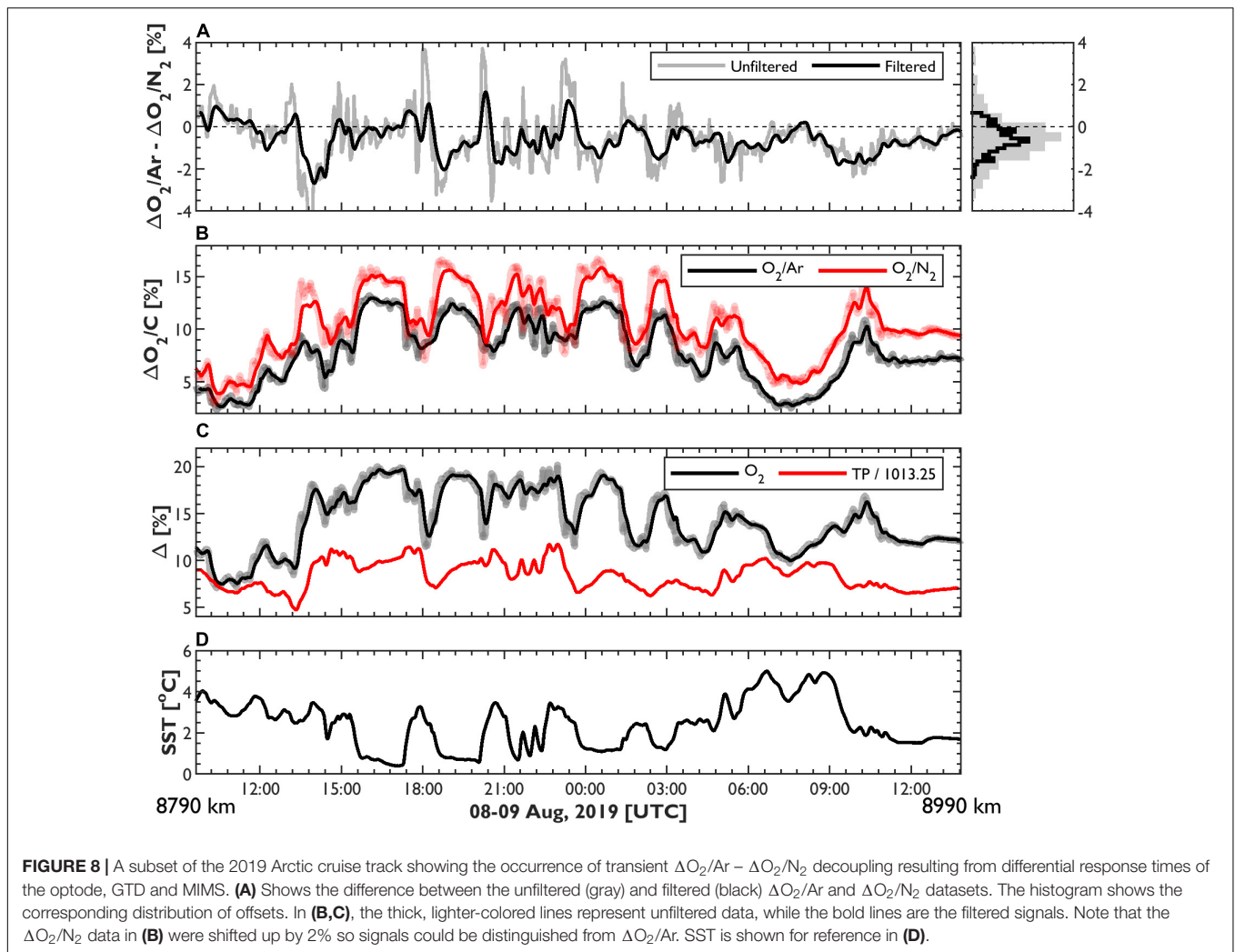
In the offshore NEP-summer waters, surface $\Delta N_2/Ar$ values of $\sim 0.25\%$ (**Supplementary Figure 4**) predominantly reflect the influence of summertime warming in increasing gas saturation states, with gas re-equilibration under low-to-moderate wind speeds (typically $< 10 m s^{-1}$) maintaining ΔN_2 greater than ΔAr . In contrast, the $\Delta N_2/Ar$ anomalies along the offshore section of the NEP-winter cruise (median $\sim 0.5\%$) likely reflect cooling and stronger bubble and, to some extent, mixing fluxes, which, respectively, lower and elevate gas saturation states and $\Delta N_2/Ar$. Despite lacking $\Delta N_2/Ar_{deep}$ observations from the winter cruise (archived observations suggest a value close to 0.5% ; Hamme et al., 2019), we estimated relatively strong offshore mixing rates ($\kappa_Z \sim 4 \times 10^{-4} m^2 s^{-1}$; **Supplementary Table 1**), implying that mixing contributed to the observed $\Delta N_2/Ar$ disequilibrium. The influence of vertical mixing was also likely significant in the QCS region, where we observed the largest $\Delta N_2/Ar$ disequilibria and negative surface ΔO_2 (**Figure 4A**). In this region, sedimentary or deep-water denitrification, which has been observed in coastal fjords and inland channels throughout British Columbia (Manning et al., 2010; Bourbonnais et al., 2013) may have elevated $\Delta N_2/Ar_{deep}$, resulting in the vertical



supply of microbially N_2 -enriched water into surface waters. This hypothesis is supported by observations of lower N^* , an indicator of nitrate loss via denitrification (Gruber and Sarmiento, 1997), in the QCS region (range ~ -2 to $-6 \mu\text{mol L}^{-1}$ in the upper 500 m), relative to offshore waters of the NEP (**Supplementary Figure 5C**). As the success of the N_2' calculations suggest (following section), the influence of vertical mixing on surface $\Delta N_2/Ar$ across all sampling regions in NEP-winter was important, and our combined estimates of κ_Z and $\Delta N_2/Ar_{deep}$ capture this process.

In the Arctic, the elevated ΔAr and ΔN_2 we observed (up to 10%; **Supplementary Figure 2**) exceed most previously reported gas observations in the region (Eveleth et al., 2014; Hamme et al., 2017). However, such conditions can be produced in mixed layer model simulations replicating the conditions encountered before our sampling in northern Baffin Bay (BB) (warming up to 9°C

over ~ 30 days and mean wind speeds $\sim 4 \text{ m s}^{-1}$; simulation results based on the model in Izett and Tortell, 2021; not shown). The resulting positive $\Delta N_2/Ar$ disequilibria we observed (median $\sim 0.5\%$ in BB; **Supplementary Figure 4**) is consistent with values of ~ 0.3 – 0.7% predicted in these numerical simulations, reflecting the dominant influence of seasonal warming. Although warming increases both ΔAr and ΔN_2 , Ar re-equilibrates more rapidly than N_2 , causing $\Delta N_2 > \Delta Ar$. The mixing contribution was less important (mean BB $\kappa_Z \sim 1 \times 10^{-4} \text{ m}^2 \text{ s}^{-1}$). Elsewhere in the Arctic, the high spatial heterogeneity of ΔO_2 , ΔAr , and ΔN_2 likely reflects variability in ice cover and environmental forcing via air-sea exchange, SST changes and mixing. Although denitrification may be significant in some Arctic waters, including the shallow shelves of the western Arctic (Reeve et al., 2019), the low $\Delta N_2/Ar_{deep}$ observed throughout our cruise region (**Supplementary Figure 5C**) suggests that the vertical



supply of microbially N_2 -enriched water into surface waters was not important in driving $\Delta O_2/Ar - \Delta O_2/N_2$ differences.

Evaluating $\Delta O_2/N_2'$ as an NCP Tracer in Field Studies

Across our three cruise dataset, biological O_2 saturation anomalies based on O_2/N_2 measurements were able to replicate the high-resolution heterogeneity in surface productivity captured by the MIMS-based $\Delta O_2/Ar$ surveys (Figures 3–5). However, offsets between $\Delta O_2/Ar$ and uncorrected $\Delta O_2/N_2$ manifested as important deviations in NCP estimates derived from the respective tracers (Figure 7). Most importantly, in a portion of the dataset (~15% of the pooled data), $\Delta O_2/N_2$ -NCP predicted net heterotrophic conditions (negative NCP), whereas $\Delta O_2/Ar$ -NCP was positive (Table 1). Notwithstanding sources of analytical errors (see above), these offsets are largely attributable to physical processes which cause ΔN_2 and ΔAr to diverge. If uncorrected, these effects can have significant consequences for the interpretation of oceanic productivity and trophic status, particularly if NCP estimates are integrated over

an annual cycle. Fortunately, such biases can be corrected to a large extent, using the new tracer $\Delta O_2/N_2'$. When we apply these corrections, derived $\Delta O_2/N_2'$ approached $\Delta O_2/Ar$ across all cruise regions and sub-regions, and the linear relationship between these tracers was not significantly different than one (Figure 6).

On regional scales, $\Delta O_2/N_2'$ -NCP was roughly equivalent to $\Delta O_2/Ar$ -NCP, and was typically more accurate than $\Delta O_2/N_2$ -NCP (Figure 7). Indeed, in all sampling sub-regions, the median difference between $\Delta O_2/Ar$ - and $\Delta O_2/N_2'$ -NCP was lower than corresponding differences with $\Delta O_2/N_2$ -NCP (Table 1). While the N_2' calculations were unable to fully eliminate NCP biases, our results nonetheless demonstrate the ability of $\Delta O_2/N_2'$ to reduce NCP estimation errors. For example, offsets between $\Delta O_2/Ar$ - and $\Delta O_2/N_2'$ -NCP (red lines in Figure 7B) were typically smaller than NCP errors associated with vertical O_2 mixing fluxes (Table 1) or the ~20–40% uncertainty in the O_2 gas transfer velocity, k_{O_2} (gray shading in Figure 7B; Bender et al., 2011; Wanninkhof, 2014). Biases in the $\Delta O_2/N_2$ -NCP dataset (black lines in Figure 7B) were often equal to or greater than these other errors. Median mixing biases, estimated from

N_2O -based measurements in the NEP (following Izett et al., 2018), or by combining NEMO model- and CTD-derived κ_Z and O_2 observations in the Arctic, ranged from ~ 2 to > 20 $\text{mmol } O_2 \text{ m}^{-2} \text{ d}^{-1}$, with higher values in nearshore regions. Errors associated with a 20% uncertainty in k_{O_2} were up to ~ 12 $\text{mmol } O_2 \text{ m}^{-2} \text{ d}^{-1}$ (mean ~ 3 $\text{mmol } O_2 \text{ m}^{-2} \text{ d}^{-1}$). Excluding observations where the $\Delta O_2/Ar - \Delta O_2/N_2$ offset was $> 1.5\%$ (i.e., likely resulting from analytical uncertainties and sampling artifacts), biases between uncorrected $\Delta O_2/N_2'$ - and $\Delta O_2/Ar$ -NCP exceeded the magnitude of the corresponding air-sea and O_2 mixing flux errors in ~ 40 and 5% of the dataset, respectively. These values were reduced to ~ 10 and 1% after applying N_2' calculations. This result suggests that uncertainty in $\Delta O_2/N_2'$ will be typically smaller than other main sources of error in NCP calculations. Moreover, $\Delta O_2/N_2'$ -NCP more frequently predicted the same metabolic status as $\Delta O_2/Ar$ -based estimates in all sub-regions ($\sim 96\%$ of all observations; **Table 1**). Taken together, these results demonstrate the strong potential of the N_2' approach for reducing biases in NCP estimates derived from O_2/N_2 surveys, even if offsets between $\Delta O_2/Ar$ and $\Delta O_2/N_2'$ cannot be fully reconciled.

Notably, the relative success the N_2' calculations varied by sub-region. In the NEP (summer and winter), $\Delta O_2/N_2'$ represented a significant improvement over uncorrected $\Delta O_2/N_2$. In parts of the Arctic, however, the benefit of N_2' is somewhat less clear, as median and pair-wise offsets between NCP calculations were similar in both the $\Delta O_2/N_2$ and $\Delta O_2/N_2'$ datasets. Yet, our analyses suggest that $\Delta O_2/N_2'$ is a less ambiguous NCP tracer, particularly in Baffin Bay where estimates based on $\Delta O_2/N_2$ had the opposite sign to $\Delta O_2/Ar$ -NCP in $\sim 5\%$ of the dataset (compared with 0% in the $\Delta O_2/N_2'$ dataset). In the coastal waters of the Arctic shelf and CAA, where the vertical O_2 mixing bias may overwhelm the ML mass balance, N_2' calculations are subject to more uncertainty, and may therefore not be necessary. Indeed, in the shelf and CAA regions, median NCP biases based on $\Delta O_2/N_2'$ and $\Delta O_2/N_2$ ($\sim 0.8 \pm 2.1$ and 1.1 ± 1.9 $\text{mmol } O_2 \text{ m}^{-2} \text{ d}^{-1}$, respectively; uncertainty represents one standard deviation around the mean value) were smaller than the mean mixing biases of $\sim 6.2 \pm 12.1$ $\text{mmol } O_2 \text{ m}^{-2} \text{ d}^{-1}$. In the nearshore waters of the NEP (QCS region), the O_2 mixing bias (up to ~ 90 $\text{mmol } O_2 \text{ m}^{-2} \text{ d}^{-1}$) constituted a major component of the ML O_2 mass balance and was higher than NCP biases between the various tracers (~ 9 $\text{mmol } O_2 \text{ m}^{-2} \text{ d}^{-1}$). However, N_2' calculations still significantly reduced the large errors between $\Delta O_2/Ar$ - and $\Delta O_2/N_2$ -NCP. Thus, while N_2' can reduce NCP errors in both coastal and offshore waters, future work will still need to address challenges relating to the vertical mixing of O_2 in such dynamic regions. In contrast, calculation of $\Delta O_2/N_2'$ will likely be necessary to accurately reflect the true metabolic state of low productivity offshore waters and evaluate seasonal changes in ocean productivity.

Remaining Biases Between $\Delta O_2/Ar$ and $\Delta O_2/N_2'$

Notwithstanding sources of measurement and analytical error (further details in **Supplementary Material Section 4**), remaining biases between $\Delta O_2/Ar$ and $\Delta O_2/N_2'$ arise from errors in $\Delta O_2/N_2'$ computations, which have been estimated by

Izett and Tortell (2021) to be $\sim 0.3\%$. That work demonstrated the ability of the N_2' budget to capture the dominant processes driving N_2 evolution in oceanic waters of the offshore NEP. In the present dataset, however, errors are most significant in nearshore regions where the negligence of lateral fluxes likely oversimplifies $\Delta N_2/Ar$ dynamics. For example, lateral advection or mixing, freshwater input and ice processes may contribute to divergence between the NCP tracers, while significant water mass transport would produce uncertainty in the environmental histories that we ascribe to our underway observations. These processes are difficult to constrain with simple modeling approaches, and the effects of sea and glacier ice melt on surface seawater $\Delta N_2/Ar$ are uncertain (Zhou et al., 2014). Moreover, as we lack broad coverage of direct κ_Z and $\Delta N_2/Ar_{\text{deep}}$ observations, misrepresentation of these terms may have contributed to errors in our $\Delta O_2/N_2'$ calculations. However, sensitivity analyses in which we set κ_Z to $0 \text{ m}^2 \text{ s}^{-1}$ or varied κ_Z and $\Delta N_2/Ar_{\text{deep}}$ (by $5 \times 10^{-5} \text{ m}^2 \text{ s}^{-1}$ and 0.25% , respectively), produced $\Delta O_2/N_2'$ -NCP estimates that were typically better than, or equivalent to, $\Delta O_2/N_2$ -based values (blue shading in **Figure 7B**), suggesting that even sparse κ_Z or $\Delta N_2/Ar_{\text{deep}}$ measurements can improve the performance of $\Delta O_2/N_2'$ as an NCP tracer. In the absence of direct observations, κ_Z may be derived from numerical simulations or geochemical (e.g., Izett et al., 2018) and hydrographic proxies (Cronin et al., 2015; Haskell et al., 2016), while $\Delta N_2/Ar_{\text{deep}}$ can be approximated using archived datasets (Hamme et al., 2019).

Future improvements in the accuracy of $\Delta O_2/N_2'$ will require further refinement of gas flux parameterizations and environmental datasets, particularly in polar regions where current reanalysis products are less accurate (**Supplementary Figure 8**), and partial ice-cover complicates air-sea flux parameterizations (Islam et al., 2016). Climatological or ancillary datasets of subsurface hydrographic conditions or MLD (e.g., from Argo floats) may be used to better evaluate the time-variability of ML gas evolution, while air-sea flux parameterizations should be validated for the relevant study region. These considerations would enable application of the present approach in unattended optode/GTD deployments from VOS or USV surveys where subsurface observations are presently not feasible.

CONCLUSION AND OUTLOOK

In this paper, we evaluated a new approach for deriving NCP estimates from underway O_2/N_2 surveys, building on the model framework presented in Izett and Tortell (2021). The current study constitutes the first published NCP results based on underway ship-board O_2/N_2 data, and a first attempt at comparing $\Delta O_2/Ar$ -NCP and $\Delta O_2/N_2$ -NCP. Our results demonstrate the potential to accurately derive NCP from underway O_2/N_2 observations obtained from optode and GTD measurements in a range of ocean regions, including coastal and offshore waters of polar and subpolar seas. These observations, combined with simple computations of the new tracer, $\Delta O_2/N_2'$, can be used to replicate $\Delta O_2/Ar$ -based NCP estimates. In

some cases, however, NCP estimates based on uncorrected $\Delta O_2/N_2$ may be sufficiently accurate, and future work should endeavor to address other current limitations in NCP calculations (e.g., vertical O_2 mixing flux biases) or further validate the present approach. In all future applications, ship-board gas sensors should be installed as near to the seawater intake as possible and routinely calibrated to optimize data accuracy. For research vessel deployments, the optode should be calibrated over a range of hydrographic conditions using discrete samples collected from the ship's seawater supply line and surface Niskin bottle (as performed in this study). This practice will minimize potential sampling artifacts related to dissolved O_2 consumption or production in the supply line (Juraneck et al., 2010). For remote applications, we recommend calibrating the optode in the laboratory before and after deployments. For all applications, the GTD should be offset-calibrated (at minimum) by comparing in-air GTD measurements with sea level pressure observations, or by assessing the instrument's accuracy in an equilibrated water sample. When possible, optode/GTD-derived $N_{2,sat}$ should be evaluated using discrete samples. Successful application of $\Delta O_2/N_2'$ will also rely on accurate parameterization of the environmental conditions for the study region of interest, and careful data handling to minimize analytical errors in the measurements of O_2/N_2 . Future work will be aided by the continued development of reanalysis data products and gas sensor technology.

Widespread application of the approach evaluated here has the potential to significantly expand global coverage of NCP measurements from relatively inexpensive autonomous surface O_2 and N_2 measurements. Indeed, we recommend that future surveys incorporate optode/GTD instrumentation or autonomous measurement systems (e.g., Izett and Tortell, 2020) into existing sampling infrastructure on research vessels, VOS (e.g., container ships, cruise ships, sailboats) and *in-situ* USVs to provide high spatial and temporal coverage of NCP estimates, and improved integration with other autonomous oceanographic and ecological observations. Given the anticipated impacts of climate change on marine biological productivity, such observations will be crucial for evaluating future variability in biogeochemical and environmental conditions, and predicting associated ecosystem-level responses across a range of oceanic environments.

DATA AVAILABILITY STATEMENT

The datasets generated and analyzed in this study are provided on Zenodo in an O2N2 NCP toolbox (<https://doi.org/10.5281/zenodo.4024925>), which includes underway and discrete gas data, and corresponding hydrographic and environmental observations. The repository also contains Matlab codes and sample calculations for some of the analyses presented in this manuscript. Underway $\Delta O_2/Ar$, O_2 and N_2 data, and corresponding hydrographic and geographic information, are also compiled at Pangaea (NEP data; <https://doi.pangaea.de/10.1594/PANGAEA.933345>) and the Polar Data Catalogue (Arctic data; <https://doi.org/10.5884/13242>). Ancillary CTD and TSG data for the NE Pacific and Arctic were provided by the Water

Properties group of the Institute of Ocean Sciences (<http://www.waterproperties.ca/linep/cruises.php>) and the Amundsen Science group of U. Laval (<https://doi.org/10.5884/12713> and <https://doi.org/10.5884/12715>). The CCMPv2 wind speed data were downloaded from <https://www.remss.com>. The NCEP/NCAR sea level pressure, NARR wind speed and NOAA OI SST reanalysis data products were obtained from <https://psl.noaa.gov/data/gridded/>. AMSR-2 sea ice data are available at <http://www.osi-saf.org/?q=content/global-sea-ice-concentration-amsr-2>.

AUTHOR CONTRIBUTIONS

RI designed the study, conducted most of the field deployments, and led the data analyses and manuscript writing. PT and RH contributed to the study conceptualization. RH, CCM, and AB conducted field sampling for discrete N_2/Ar data, while RH and AB performed the analyses on the discrete samples and provided the resulting data. CM provided assistance with the planning of field deployments and contributed to the analyses of the GTD data. CCM and PT assisted during field deployments. PT provided funding for the work, and contributed significantly to the manuscript writing. All other authors provided feedback on the manuscript writing and structure.

FUNDING

This work was supported by the Natural Sciences and Engineering Research Council of Canada (NSERC) through a Discovery Grant (PT), an Alexander Graham Bell Canada Graduate Scholarship (RI), and postdoctoral fellowship (CCM). Funding was also provided by the ArcticNet and MEOPAR Networks of Centres of Excellence Canada, through grants to PT, and Polar Knowledge Canada through a Northern Science Training Program grant to RI.

ACKNOWLEDGMENTS

We would like to thank Susan Allen, Debby Ianson, Laurie Juraneck, and two reviewers for their insightful comments on this work. We also thank William Burt, Ross McCulloch, Zarah Zheng, and Holly Westbrook for their assistance collecting field data, and Mark Belton, Erinn Raftery, and Darcy Perin for their assistance analyzing discrete O_2 and N_2/Ar samples. Finally, we wish to thank Marie Robert, many scientists from the Institute of Ocean Sciences and Amundsen Science group, and the Captain and crews of the CCGS Tully and CCGS Amundsen for their significant support during field sampling.

SUPPLEMENTARY MATERIAL

The Supplementary Material for this article can be found online at: <https://www.frontiersin.org/articles/10.3389/fmars.2021.718625/full#supplementary-material>

REFERENCES

- Amundsen Science Data Collection (2020a). *CTD-Rosette Data Collected by the CCGS Amundsen in the Canadian Arctic. Arcticnet Inc., arcticnet Inc., Québec, Canada. Processed data. Version 1.* Waterloo: Canadian Cryospheric Information Network (CCIN), doi: 10.5884/12713
- Amundsen Science Data Collection (2020b). *TSG Data Collected by the CCGS Amundsen in the Canadian Arctic. Arcticnet Inc., Arcticnet Inc., Québec, Canada. Processed data. Version 1.* Waterloo: Canadian Cryospheric Information Network (CCIN), doi: 10.5884/12715
- Atlas, R., Hoffman, R. N., Ardizzone, J., Leidner, S. M., Jusem, J. C., Smith, D. K., et al. (2011). A cross-calibrated, multiplatform ocean surface wind velocity product for meteorological and oceanographic applications. *Bull. Am. Meteorol. Soc.* 92, 157–174. doi: 10.1175/2010BAMS2946.1
- Bender, M. L., Kinter, S., Cassar, N., and Wanninkhof, R. (2011). Evaluating gas transfer velocity parameterizations using upper ocean radon distributions. *J. Geophys. Res.* 116, 1–11. doi: 10.1029/2009JC005805
- Bittig, H. C., Körtzinger, A., Neill, C., van Ooijen, E., Plant, J. N., Hahn, J., et al. (2018). Oxygen optode sensors: principle, characterization, calibration, and application in the ocean. *Front. Mar. Sci.* 4:429. doi: 10.3389/fmars.2017.00429
- Bourbonnais, A., Lehmann, M. F., Hamme, R. C., Manning, C. C., and Juniper, S. K. (2013). Nitrate elimination and regeneration as evidenced by dissolved inorganic nitrogen isotopes in Saanich Inlet, a seasonally anoxic fjord. *Mar. Chem.* 157, 194–207. doi: 10.1016/j.marchem.2013.09.006
- Bushinsky, S. M., and Emerson, S. (2015). Marine biological production from in situ oxygen measurements on a profiling float in the subarctic Pacific Ocean. *Glob. Biogeochem. Cycles* 29, 2050–2060. doi: 10.1002/2015GB005251
- Butterworth, B. J., and Miller, S. D. (2016). Air-sea exchange of carbon dioxide in the Southern Ocean and Antarctic marginal ice zone. *Geophys. Res. Lett.* 43, 7223–7230. doi: 10.1002/2016GL069581
- Castro de la Guardia, L., Garcia-Quintana, Y., Claret, M., Hu, X., Galbraith, E. D., and Myers, P. G. (2019). Assessing the role of high-frequency winds and sea ice loss on arctic phytoplankton blooms in an ice-ocean-biogeochemical model. *J. Geophys. Res. Biogeosci.* 124, 2728–2750. doi: 10.1029/2018JG004869
- Craig, H., and Hayward, T. (1987). Oxygen supersaturation in the ocean: biological versus physical contributions. *Science* 235, 199–202. doi: 10.1126/science.235.4785.199
- Cronin, M. F., Pellan, N. A., Emerson, S. R., and Crawford, W. R. (2015). Estimating diffusivity from the mixed layer heat and salt balances in the North Pacific. *J. Geophys. Res. Ocean* 120, 7346–7362. doi: 10.1002/2015JC011010
- D'Asaro, E., and McNeil, C. (2008). Air-sea gas exchange at extreme wind speeds measured by autonomous oceanographic floats. *J. Mar. Syst.* 74, 722–736. doi: 10.1016/j.jmarsys.2008.02.006
- D'Asaro, E. A., and McNeil, C. (2013). Calibration and stability of oxygen sensors on autonomous floats. *J. Atmos. Ocean. Technol.* 30, 1896–1906. doi: 10.1175/JTECH-D-12-00222.1
- Emerson, S. (2014). Annual net community production and the biological carbon flux in the ocean. *Global Biogeochem. Cycles* 28, 14–28. doi: 10.1002/2013GB004680
- Emerson, S., and Bushinsky, S. (2016). The role of bubbles during air-sea gas exchange. *J. Geophys. Res. Ocean* 121, 4360–4376. doi: 10.1002/2016JC011744
- Emerson, S., and Stump, C. (2010). Net biological oxygen production in the ocean-II: remote in situ measurements of O_2 and N_2 in subarctic Pacific surface waters. *Deep Sea Res. 1 Oceanogr. Res. Pap.* 57, 1255–1265. doi: 10.1016/j.dsr.2010.06.001
- Emerson, S., Stump, C., Wilbur, D., and Quay, P. (1999). Accurate measurement of O_2 , N_2 , and Ar gases in water and the solubility of N_2 . *Mar. Chem.* 64, 337–347. doi: 10.1016/S0304-4203(98)00090-5
- Eveleth, R., Cassar, N., Sherrell, R. M., Ducklow, H., Meredith, M. P., Venables, H. J., et al. (2017). Ice melt influence on summertime net community production along the Western Antarctic Peninsula. *Deep Sea Res. 2 Oceanogr. Res. Pap.* 139, 89–102. doi: 10.1016/j.dsr.2.2016.07.016
- Eveleth, R., Timmermans, M.-L., and Cassar, N. (2014). Physical and biological controls on oxygen saturation variability in the upper Arctic Ocean. *J. Geophys. Res. Ocean* 119, 7420–7432. doi: 10.1002/2014JC009816
- Garcia, H. E., and Gordon, L. I. (1992). Oxygen solubility in seawater: better fitting equations. *Limnol. Oceanogr.* 37, 1307–1312. doi: 10.2307/2837876
- Garcia, H. E., and Gordon, L. I. (1993). Erratum: oxygen solubility in seawater: better fitting equations. *Limnol. Oceanogr.* 38:656.
- Gruber, N., and Sarmiento, J. L. (1997). Global patterns of marine nitrogen fixation and denitrification. *Glob. Biogeochem. Cycles* 11, 235–266.
- Hamme, R. C., Berry, J. E., Klymak, J. M., and Denman, K. L. (2015). In situ O_2 and N_2 measurements detect deep-water renewal dynamics in seasonally-anoxic Saanich Inlet. *Cont. Shelf Res.* 106, 107–117. doi: 10.1016/j.csr.2015.06.012
- Hamme, R. C., and Emerson, S. R. (2004). The solubility of neon, nitrogen and argon in distilled water and seawater. *Deep Sea Res. 1 Oceanogr. Res. Pap.* 51, 1517–1528. doi: 10.1016/j.dsr.2004.06.009
- Hamme, R. C., and Emerson, S. R. (2006). Constraining bubble dynamics and mixing with dissolved gases: Implications for productivity measurements by oxygen mass balance. *J. Mar. Res.* 64, 73–95. doi: 10.1357/002224006776412322
- Hamme, R. C., Emerson, S. R., Severinghaus, J. P., Long, M. C., and Yashayaev, I. (2017). Using Noble gas measurements to derive air-sea process information and predict physical gas saturations. *Geophys. Res. Lett.* 44, 9901–9909. doi: 10.1002/2017GL075123
- Hamme, R. C., Nicholson, D. P., Jenkins, W. J., and Emerson, S. R. (2019). Using Noble Gases to Assess the Ocean's Carbon Pumps. *Ann. Rev. Mar. Sci.* 11, 1–29. doi: 10.1146/annurev-marine-121916-063604
- Haskell, W. Z., Prokopenko, M. G., Stanley, R. H. R., and Knapp, A. N. (2016). Estimates of vertical turbulent mixing used to determine a vertical gradient in net and gross oxygen production in the oligotrophic South Pacific Gyre. *Geophys. Res. Lett.* 43, 7590–7599. doi: 10.1002/2016GL069523
- Islam, F., DeGrandpre, M., Beatty, C., Krishfield, R., and Toole, J. (2016). Gas exchange of CO_2 and O_2 in partially ice-covered regions of the Arctic Ocean investigated using in situ sensors. *IOP Conf. Ser. Earth Environ. Sci.* 35:012018. doi: 10.1088/1755-1315/35/1/012018
- Izett, R. (2021). *O2N2 NCP Toolbox (Version 2021.04)*. doi: 10.5281/zenodo.4024925.
- Izett, R., Manning, C. C., Hamme, R. C., and Tortell, P. D. (2018). Refined estimates of net community production in the Subarctic Northeast Pacific derived from $\Delta O_2/Ar$ measurements with N_2O -based corrections for vertical mixing. *Glob. Biogeochem. Cycles* 32, 326–350. doi: 10.1002/2017GB005792
- Izett, R., and Tortell, P. (2020). The pressure of in situ gases instrument (PIGI) for autonomous shipboard measurement of dissolved O_2 and N_2 in surface ocean waters. *Oceanography* 33, 13–15. doi: 10.5670/oceanog.2020.214
- Izett, R., and Tortell, P. (2021). $\Delta O_2/N_2'$ as a tracer of mixed layer net community production: theoretical considerations and proof-of-concept. *Limnol. Oceanogr. Methods* 1–13. doi: 10.1002/lom3.10440
- Juranek, L., Takahashi, T., Mathis, J., and Pickart, R. (2019). Significant biologically mediated CO_2 uptake in the Pacific Arctic during the late open water season. *J. Geophys. Res. Ocean* 124, 1–23. doi: 10.1029/2018JC014568
- Juranek, L. W., Hamme, R. C., Kaiser, J., Wanninkhof, R., and Quay, P. D. (2010). Evidence of O_2 consumption in underway seawater lines: implications for air-sea O_2 and CO_2 fluxes. *Geophys. Res. Lett.* 37, 1–5. doi: 10.1029/2009GL040423
- Kaiser, J., Reuer, M. K., Barnett, B., and Bender, M. L. (2005). Marine productivity estimates from continuous O_2/Ar ratio measurements by membrane inlet mass spectrometry. *Geophys. Res. Lett.* 32, 1–5. doi: 10.1029/2005GL023459
- Kalnay, E., Kanamitsu, M., Kistler, R., Collins, W., Deaven, D., Gandin, L., et al. (1996). The NCEP/NCAR 40-year reanalysis project. *Bull. Am. Meteorol. Soc.* 77, 437–471. doi: 10.1175/1520-04771996077<0437:TNYRP>2.0.CO;2
- Kana, T. M., Darkangelo, C., Hunt, M. D., Oldham, J. B., Bennett, G. E., and Cornwell, J. C. (1994). Membrane inlet mass spectrometer for rapid high-precision determination of N_2 , O_2 , and Ar in environmental water samples. *Anal. Chem.* 66, 4166–4170. doi: 10.1021/ac00095a009
- Kavanaugh, M. T., Emerson, S. R., Hales, B., Lockwood, D. M., Quay, P. D., and Letelier, R. M. (2014). Physicochemical and biological controls on primary and net community production across northeast Pacific seascapes. *Limnol. Oceanogr.* 59, 2013–2027. doi: 10.4319/lo.2014.59.6.2013
- Liang, J.-H. H., Deutsch, C., McWilliams, J. C., Baschek, B., Sullivan, P. P., and Chiba, D. (2013). Parameterizing bubble-mediated air-sea gas exchange and its effect on ocean ventilation. *Glob. Biogeochem. Cycles* 27, 894–905. doi: 10.1002/gbc.20080
- Manning, C. C., Hamme, R. C., and Bourbonnais, A. (2010). Impact of deep-water renewal events on fixed nitrogen loss from seasonally-anoxic Saanich Inlet. *Mar. Chem.* 122, 1–10. doi: 10.1016/j.marchem.2010.08.002

- McNeil, C., Katz, D., Wanninkhof, R., and Johnson, B. (2005). Continuous shipboard sampling of gas tension, oxygen and nitrogen. *Deep Sea Res. Part 1 Oceanogr. Res. Pap.* 52, 1767–1785. doi: 10.1016/j.dsr.2005.04.003
- Mesinger, F., DiMego, G., Kalnay, E., Mitchell, K., Shafran, P. C., Ebisuzaki, W., et al. (2006). North American regional reanalysis. *Bull. Am. Meteorol. Soc.* 87, 343–360. doi: 10.1175/BAMS-87-3-343
- Moore, J. K., Fu, W., Primeau, F., Britten, G. L., Lindsay, K., Long, M., et al. (2018). Sustained climate warming drives declining marine biological productivity. *Science* 359, 1139–1143. doi: 10.1126/science.aao6379
- Palevsky, H., and Nicholson, D. (2018). The North Atlantic biological pump: insights from the ocean observatories initiative Irminger Sea Array. *Oceanography* 31, 42–49. doi: 10.5670/oceanog.2018.108
- Reeve, J. L., Hamme, R. C., and Williams, W. J. (2019). Tracing denitrification in the Canada Basin: N_2 loss to the atmosphere on the Chukchi Shelf and benthic inputs in deep waters. *Deep Sea Res. Part 1 Oceanogr. Res. Pap.* 143, 127–138. doi: 10.1016/j.dsr.2018.11.003
- Reynolds, R. W., Smith, T. M., Liu, C., Chelton, D. B., Casey, K. S., and Schlax, M. G. (2007). Daily high-resolution-blended analyses for sea surface temperature. *J. Clim.* 20, 5473–5496.
- Spreen, G., Kaleschke, L., and Heygster, G. (2008). Sea ice remote sensing using AMSR-E 89-GHz channels. *J. Geophys. Res.* 113:C02S03. doi: 10.1029/2005JC003384
- Steiner, N., Vagle, S., Denman, K. L., and McNeil, C. (2007). Oxygen and nitrogen cycling in the northeast Pacific - simulations and observations at Station Papa in 2003/2004. *J. Mar. Res.* 65, 441–469. doi: 10.1357/002224007781567658
- Teeter, L., Hamme, R. C., Ianson, D., and Bianucci, L. (2018). Accurate estimation of net community production from O_2/Ar measurements. *Glob. Biogeochem. Cycles* 32, 1163–1181. doi: 10.1029/2017GB005874
- Thomson, R. E., and Fine, I. V. (2003). Estimating mixed layer depth from oceanic profile data. *J. Atmos. Ocean. Technol.* 20, 319–329. doi: 10.1175/1520-04262003020<0319:EMLDFO>2.0.CO;2
- Tortell, P. D. (2005). Dissolved gas measurements in oceanic waters made by membrane inlet mass spectrometry. *Limnol. Oceanogr. Methods* 3, 24–37. doi: 10.4319/lom.2005.3.24
- Uchida, H., Kawano, T., Kaneko, I., and Fukasawa, M. (2008). In situ calibration of optode-based oxygen sensors. *J. Atmos. Ocean. Technol.* 25, 2271–2281. doi: 10.1175/2008JTECHO549.1
- Vagle, S., McNeil, C., and Steiner, N. (2010). Upper ocean bubble measurements from the NE Pacific and estimates of their role in air-sea gas transfer of the weakly soluble gases nitrogen and oxygen. *J. Geophys. Res. Ocean* 115, 1–16. doi: 10.1029/2009JC005990
- Volk, T., and Hoffert, M. I. (1985). “Ocean carbon pumps: analysis of relative strengths and efficiencies in ocean-driven atmospheric CO_2 changes,” in *The Carbon Cycle and Atmospheric CO_2 : Natural Variations Archean to Present*, eds E. T. Sundquist and W. S. Broecker (Washington, DC: American Geophysical Union), 99–110.
- Wanninkhof, R. (2014). Relationship between wind speed and gas exchange over the ocean revisited. *Limnol. Oceanogr. Methods* 12, 351–362. doi: 10.1029/92JC00188
- Ware, D. M., and Thomson, R. E. (2005). Bottom-up ecosystem trophic dynamics determine fish production in the Northeast Pacific. *Science* 308, 1280–1284. doi: 10.1126/science.1109049
- Zhou, J., Delille, B., Brabant, F., and Tison, J. L. (2014). Insights into oxygen transport and net community production in sea ice from oxygen, nitrogen and argon concentrations. *Biogeosciences* 11, 5007–5020. doi: 10.5194/bg-11-5007-2014

Conflict of Interest: CM discloses a financial interest as vice president of Pro-Oceanus Systems Inc.

The remaining authors declare that the research was conducted in the absence of any commercial or financial relationships that could be construed as a potential conflict of interest.

Publisher’s Note: All claims expressed in this article are solely those of the authors and do not necessarily represent those of their affiliated organizations, or those of the publisher, the editors and the reviewers. Any product that may be evaluated in this article, or claim that may be made by its manufacturer, is not guaranteed or endorsed by the publisher.

Copyright © 2021 Izett, Hamme, McNeil, Manning, Bourbonnais and Tortell. This is an open-access article distributed under the terms of the Creative Commons Attribution License (CC BY). The use, distribution or reproduction in other forums is permitted, provided the original author(s) and the copyright owner(s) are credited and that the original publication in this journal is cited, in accordance with accepted academic practice. No use, distribution or reproduction is permitted which does not comply with these terms.